enlarged spleen and lymph nodes (LNs) together with increased numbers of myeloid cells, plasma cells, and Mott cells (18–20). In addition, *me/me* and me^v/me^v mice (hereafter both referred to as *motheaten* mice) experience chronic inflammation and systemic autoimmune disease, as evidenced by hypergammaglobulinemia, high titers of autoantibodies, and immune complex deposition with consequent tissue damage (20). As a result, the mutant animals die of interstitial pneumonitis at ~2–3 wk (*me/me*) or 9–12 wk (me^v/me^v) of age (18, 19). The functional abnormality of DCs in *motheaten* mice has remained uncharacterized, but the number of DCs in these animals is markedly increased in lung, liver, and kidney, suggesting a role for Shp1 in negative regulation of DC proliferation and differentiation (21).

It is difficult to distinguish between DC-intrinsic and DC-extrinsic effects of Shp1 deficiency in *motheaten* mice, however, given that the enzyme is ablated in all somatic cells. In addition, examination of the effects of an inhibitor of Shp1 or of RNA interference-mediated knockdown of Shp1 has indicated that Shp1 is an intrinsic but negative regulator of DC functions including the production of proinflammatory cytokines, migration to draining LNs, and the control of many facets of T cell-mediated immune responses (22). The precise role of Shp1 in the regulation of DC functions, especially in vivo, has however remained unclear. To address this issue, we have now generated and analyzed DC-specific Shp1 conditional knockout (CKO) mice.

Materials and Methods

Abs and reagents

A rat mAb to mouse CD16/32 (2.4G2) was prepared from the culture supernatants of hybridoma cells (kindly provided by K. Okumura, Juntendo University, Tokyo, Japan). Rabbit polyclonal antibodies (pAbs) to Shp1 were obtained from Santa Cruz Biotechnology (Santa Cruz, CA). A mouse mAb to β-tubulin (TUB2.1) as well as LPS and FITC isomer I were from Sigma-Aldrich (St. Louis, MO). HRP-conjugated goat pAbs to rabbit or mouse IgG as well as Cy3-conjugated goat pAbs to rat IgG were obtained from Jackson ImmunoResearch (West Grove, PA). A mouse mAb to phosphotyrosine (4G10) was obtained from Millipore (Billerica, MA). Pyrrolidine dithiocarbamate (PDTC), JSH-23, SB203580, wortmannin, and PP2 were obtained from Merck (Darmstadt, Germany). SP600125 or bisindolylmaleimide I was from Wako (Osaka, Japan) or Cell Signaling Technology (Danvers, MA), respectively. FITC-conjugated mAbs to mouse CD8α (53-6.7), CD62L (MEL-14), CD5 (53-7.3), CD4 (RM4-5), and IFN-γ (XMG1.2); PE-conjugated mAbs to mouse IL-17A (TC11-18H10), IL-4 (11B11), B220 (RA3-6B2), CD21/35 (7G6), and Gr-1 (Rb6-8C5); PE- or biotin-conjugated rat IgG to trinitrophenol (isotype control); an allophycocyanin-conjugated mAb to mouse CD11c (HL3); a PE–Cy7–conjugated mAb to mouse CD4 (RM4-5); biotin-conjugated mAb to mouse CD4 (RM4-5) and CD40 (3/23); PE-conjugated streptavidin; and allophycocyanin-conjugated streptavidin were obtained from BD Biosciences (San Jose, CA). FITC-conjugated mouse IgG to trinitrophenol (eBM2a, isotype control) and an mAb to Thy1.2 (30-H12), a PE-conjugated mAb to mouse CD8α (53-6.7), and CD69 (H1.2F3), an allophycocyanin-conjugated mAb to mouse Foxp3 (FJK-16s), and biotin-conjugated mAbs to mouse CD80 (16-10A1), CD86 (GL1), CD70 (FR70), Thy1.2 (30-H12), CD23 (B3B4), CD25 (PC61), TER119 (TER-119), CCR7 (4B12), and MHC class II (M5/114.15.2) were obtained from eBioscience (San Diego, CA). A PE-conjugated mAb to mouse F4/80 (BM8) was from Caltag (Burlingame, CA). An allophycocyanin-conjugated mAb to mouse CD44 (IM7); an allophycocyanin/Cy7-cojugated mAb to mouse B220 (RA3-6B2); PE/Cy7-conjugated mAb to AA4.1; and a biotin-conjugated mAb to mouse CD19 (6D5) and F4/80 (BM8) were obtained from BioLegend (San Diego, CA). Microbeads conjugated with Abs to mouse CD11c (N418) or to CD4 (L3T4) or with anti-biotin were obtained from Miltenyi Biotech (Bergisch Gladbach, Germany). HRP-conjugated (or nonconjugated) goat pAbs to mouse IgA, IgG1, IgG2a, IgG2b, and IgG3 were obtained from Bethyl Laboratories (Montgomery, TX). Rabbit pAbs to mouse IgM and HRP-conjugated goat pAbs to mouse IgM were from Zymed (South San Francisco, CA). Cy3-conjugated goat pAbs to mouse IgG were obtained from Jackson ImmunoResearch. FITC-conjugated rabbit pAbs to C3 were obtained from Abcam (Cambridge, U.K.). RPMI 1640 medium (Sigma-Aldrich) was supplemented with 10% heat-inactivated FCS, 50 μM 2-ME, 2 mM L-glutamine, 10 mM HEPES–NaOH (pH 7.4), penicillin (100 U/ml), streptomycin (100 μg/ml), and 1 mM sodium pyruvate to yield complete medium.

Animals

CD11c-*cre* mice were generated as described previously (23) and were obtained from The Jackson Laboratory (Bar Harbor, ME). They were crossed with $Ptpn6^{fl/fl}$ mice, which were generated as described previously (24), and the resulting $Ptpn6^{fl/fl}$; CD11c-*cre* (Shp1 CKO) descendants and their sex- and age-matched $Ptpn6^{fl/fl}$ littermates (controls) were studied. OT-II TCR transgenic mice ($H\text{-}2^b$), originally generated as described (25), were kindly provided by T. Hirano (RIKEN, Yokohama, Japan). Mice were bred and maintained at the Institute of Experimental Animal Research of Gunma University under specific pathogen-free conditions and were handled in accordance with the animal care guidelines of Gunma University.

Detection of deleted and floxed alleles of Ptpn6 by PCR

Splenocytes were stained with an FITC-conjugated mAb to mouse CD3ε, a PE-conjugated mAb to mouse B220, an allophycocyanin-conjugated mAb to mouse CD11c, an allophycocyanin–Cy7–conjugated mAb to mouse B220, and propidium iodide (PI). $CD11c^{high}B220^-$ conventional dendritic cells (cDCs), $CD11c^{int}B220^+$ plasmacytoid dendritic cells (pDCs), $CD11c^-CD3^+B220^-$ T cells, and $CD11c^-CD3^-B220^+$ B cells were then sorted with the use of the FACSAriaII instrument. The purity of the isolated cells was >98% for cDCs, >91% for pDCs, and >99% for T and B cells, as determined by flow cytometry. Genomic DNA was isolated from each cell population with the use of a DNeasy kit (Qiagen, Valencia, CA). Floxed (~550-bp product) and deleted (~330-bp product) *Ptpn6* alleles were then identified by PCR with SHCP27 (5′-ACCCTCCAGCTCC-TCTTC-3′), SHCP29 (5′-TGAGGTCCCGGTGAAACC-3′), and SHCP32 (5′-TGTTATGCATGTGTGTATCG-3′) primers as described previously (24). The intensities of PCR bands were determined by densitometric analysis with ImageJ software (National Institutes of Health). Deletion efficiency in each cell population was determined as the intensity of the deleted allele expressed as a percentage of that of the floxed allele plus that of the deleted allele.

Immunoblot analysis

For immunoblot analysis, cells were homogenized on ice in a lysis buffer [20 mM Tris-HCl (pH 7.6), 140 mM NaCl, 1 mM EDTA, 1% Nonidet P-40] containing 1 mM PMSF, aprotinin (10 μg/ml), and 1 mM sodium vanadate. The lysates were centrifuged at 10,000 × *g* for 15 min at 4°C, and the resulting supernatants were subjected to SDS- PAGE followed by immunoblot analysis with various Abs. Immunoreactive bands were then detected with an ECL detection system (GE Healthcare, Little Chalfont, U.K.) and an LAS 3000 image analyzer (Fujifilm, Tokyo, Japan). The intensity of bands was determined by densitometric analysis with the use of Image Gauge 4.0 software (Fujifilm).

Cell preparation and flow cytometry

For analysis or preparation of DCs or $F4/80^+$ macrophages from the spleen, peripheral LNs, or thymus (26, 27), tissue was minced with the use of forceps and then digested with collagenase (Wako, Osaka, Japan) at 400 U/ml in the presence of 5 mM EDTA (Sigma) for 30 min at 37°C. The undigested fibrous material was removed by filtration through a 70-μm cell strainer (BD Falcon, San Jose, CA), and RBCs in the filtrate were lysed with Gey's solution. The remaining cells were washed twice with PBS. $CD11c^+$ or $F4/80^+$ cells were further isolated from splenocytes with the use of anti-CD11c microbeads or anti-F4/80 biotin and anti-biotin microbeads and a MACS column (Miltenyi Biotec). The purity of the isolated $CD11c^+$ DCs or $F4/80^+$ macrophages was >95% as determined by flow cytometry.

For analysis of T and B cells in the spleen, the tissue was gently ground with autoclaved frosted glass slides in PBS, and the released cells were exposed to Gey's solution and then washed twice with PBS. For isolation of B cells, splenocytes were incubated consecutively with a biotin-conjugated mAb to CD19 and anti-biotin microbeads and were then fractionated with a MACS column. For isolation of total T cells or $CD4^+$ T cells, splenocytes were filtered through nylon wool. Cells in the filtrate were then incubated either consecutively with a biotin-conjugated mAb to Thy1.2 and anti-biotin microbeads or with anti-CD4 microbeads, respectively, before fractionation with a MACS column. The purity of the isolated B cells, $Thy1.2^+$ T cells, or $CD4^+$ T cells was >95% as determined by flow cytometry.

For flow cytometric analysis, cells were first incubated with an mAb specific for mouse CD16/32 to prevent nonspecific binding of labeled mAbs to FcγRs and were thereafter labeled with specific mAbs. Cells isolated

from each tissue were then subjected to flow cytometry with the use of a FACSCalibur or FACSAriaII instrument (BD Biosciences), and all data were analyzed with FlowJo software (Tree Star, Ashland, OR).

Immunohistofluorescence analysis

The spleen was embedded in OCT compound (Sakura Fine Technical, Tokyo, Japan) and rapidly frozen in liquid nitrogen. Cryostat sections with a thickness of 7 μm were then prepared, fixed with methanol, and stained with an FITC-conjugated mAb to B220 or to Thy1.2 as well as with a biotin-conjugated mAb to CD11c and Cy3-conjugated streptavidin. Conventional fluorescence or bright-field images were acquired with a BX-51 microscope equipped with ×10/0.4 and a ×4/0.16 objective lenses, a DP71 camera (Olympus, Tokyo, Japan), and DP controller software (Olympus) and were processed with Adobe Photoshop 7.0 software (Adobe Systems, San Jose, CA). Quantitative analysis of spleen images or for glomerular pathology was performed by the use of ImageJ software (National Institutes of Health).

Histopathology

Mice were perfused transcardially with 4% paraformaldehyde in PBS, after which tissues were removed, embedded in paraffin, and sectioned for staining with Mayer's H&E. For detection of immune complex deposition, cryostat sections (thickness, 7 μm) of the kidney were prepared, fixed with ice-cold acetone, and stained with a Cy3-conjugated pAb to mouse IgG or with FITC-conjugated pAbs to C3. Conventional fluorescence images were obtained as described earlier.

FITC sensitization

Sensitization of the skin with FITC to determine the migration of cutaneous DCs to draining LNs was performed as described previously (28). In brief, FITC isomer I was dissolved in a 50/50 (v/v) acetone/dibutylphthalate mixture immediately before application. Mice were painted on the shaved thorax and abdomen with 200 μl 1% FITC solution or vehicle alone. After 24 h, the inguinal and axillary LNs were isolated and digested with collagenase as described earlier. Cells were washed and then stained first with a biotin-conjugated mAb to mouse MHC class II and then with PE-conjugated streptavidin. The cells were washed again, stained with PI, and then analyzed by flow cytometry.

Ag uptake and processing

For analysis of the uptake and processing of OVA by DCs, splenic $CD11c^+$ DCs were isolated as described earlier and cultured with DQ-OVA (Invitrogen, Carlsbad, CA) at 100 ng/ml in complete medium for 0 to 120 min at 37°C or 4°C. DQ-OVA is a self-quenched conjugate of OVA that exhibits bright-green fluorescence after its proteolytic degradation. The cells were then washed with ice-cold PBS and analyzed by flow cytometry.

Proliferation of T cells from OT-II mice

For assay of the proliferation of T cells from OT-II mice in vitro (26), 12- to 16-wk-old Shp1 CKO and control mice were injected intravenously with 3 mg OVA (Calbiochem, San Diego, CA). After 12 h, $CD11c^+$ DCs were purified from the spleen and cultured for 72 h at various densities with OT-II $CD4^+$ T cells (1×10^5 cells per well) in 96-well, round-bottom microplates; the final 12 h of culture was performed in the additional presence of [^{3}H]thymidine (TdR) at 1 μCi per well, and the cell-associated radioactivity was subsequently measured with a scintillation spectrometer (Top Count NXT; PerkinElmer, Norwalk, CT). Culture supernatants were also assayed for IFN-γ and IL-17 with ELISA kits (R&D Systems, Minneapolis, MN).

Assay of TLR-induced cytokine production by splenic DCs

$CD11c^+$ cells (1×10^5 per well of 96-well, flat-bottom microplates) isolated from the spleens of 12- to 16-wk-old mice were cultured for 24 h in RPMI complete medium in the absence or presence of LPS (1 μg/ml). Culture supernatants were then assayed for TNF-α, IL-12 (p40), IL-1β, IL-6, IL-10, and IFN-β with ELISA kits (R&D Systems).

Intracellular cytokine staining

The intracellular expression of IL-17, IL-4, and IFN-γ in $CD4^+$ T cells was analyzed as described previously (29) with minor modifications. In brief, splenocytes were cultured for 4 h with PMA (100 ng/ml) and ionomycin (1 μg/ml), with GolgiPlug (BD Biosciences) being added at 1 μg/ml for the last 2 h. The cells were stained consecutively with a biotin-conjugated mAb to CD4 and allophycocyanin-conjugated streptavidin, fixed with 4% paraformaldehyde, and permeabilized with the use of a Cytofix/Cytoperm kit (BD Biosciences). Intracellular cytokine staining was performed with a PE-conjugated mAb to IL-17A or to IL-4 and with an FITC-conjugated mAb to IFN-γ, and the cells were then analyzed by flow cytometry.

Assay of serum Ig, anti-nuclear Abs, and anti-dsDNA

Serum was diluted 1:200 to 1:16,000, added to 96-well flat-bottom microplates coated with Abs to mouse IgM, IgG1, IgG2a, IgG2b, IgG3, or IgA, and allowed to react at 37°C for 2 h. The wells were washed and then incubated with 100 μl of a 1:4000 to 1:80,000 dilution of corresponding HRP-conjugated Abs to mouse IgM, IgG1, IgG2a, IgG2b, IgG3, or IgA at 37°C for 1 h. A tetramethylbenzidine substrate reagent set (BD Pharmingen, San Diego, CA) was used to develop the plates, and the reaction was terminated with stop solution (BD Pharmingen). Absorbance at 450 nm was measured with a microplate reader (MTP-500; Colona Electric, Tokyo, Japan). For measurement of the concentration of anti-nuclear antibodies (ANA) or anti-dsDNA Abs (IgG isotype), serum was diluted 1:100 to 1:500 and assayed with the use of an ANA ELISA kit (Alpha Diagnostics, San Antonio, TX) or anti-dsDNA mouse ELISA kit (Shibayagi, Shibukawa, Japan), respectively.

Statistical analysis

Data are presented as means ± SE and were analyzed with Student *t* test. A p value of <0.05 was considered statistically significant.

Results

Generation of DC-specific Shp1 CKO mice

To examine the impact of Shp1 ablation in DCs, we crossed mice homozygous for a floxed *Ptpn6* allele (24) with mice harboring a transgene for Cre recombinase under the control of the CD11c gene promoter (CD11c-*cre*) (23). Mouse spleen harbors two major subtypes of DCs: $CD11c^{high}$ cDCs and pDCs, the latter of which are defined as $CD11c^{int}B220^+$ cells and produce type I IFNs in response to viral and bacterial pathogens (1, 30). To evaluate the specificity and efficiency of *Ptpn6* deletion in $Ptpn6^{fl/fl}$; CD11c-*cre* (Shp1 CKO) mice at 12–20 wk of age, we isolated genomic DNA from sorted leukocyte populations, including cDCs, pDCs, T cells, and B cells of the spleen, and subjected it to semiquantitative PCR analysis. Consistent with the results of previous studies with the CD11c-*cre* transgene (31, 32), 94 or 79% of $Ptpn6^{fl}$ alleles were deleted in cDCs or pDCs, respectively, of Shp1 CKO mice, whereas only 11 and 4% of the floxed alleles were deleted in T and B cells, respectively (Fig. 1A). Immunoblot analysis also showed that the abundance of Shp1 protein in $CD11c^+$ DCs from the spleen of Shp1 CKO mice was reduced to 10% of that apparent for $Ptpn6^{fl/fl}$ (control) mice, whereas it was not significantly decreased in T, B cells, or $F4/80^+$ macrophages (Fig. 1B). These results thus indicated that the CD11c-*cre* transgene directs both the efficient and specific deletion of the Shp1 gene in $CD11c^+$ DCs.

Importance of Shp1 in DCs for homeostatic regulation of hematopoietic cells in the spleen

Shp1 CKO mice were born apparently healthy, survived to adulthood, and were fertile. They also did not manifest the typical phenotype of *motheaten* mice, characterized by retarded growth, alopecia, and inflammation of the paws (18, 19) (Supplemental Fig. 1). However, Shp1 CKO mice did manifest marked splenomegaly (Fig. 2A). At 12 and 24 wk of age, the weight of the spleen of Shp1 CKO mice was about twice that of the spell of control animals (Fig. 2B). Indeed, the total number of splenocytes as well as the numbers of splenic B cells and $CD4^+$ T cells in Shp1 CKO mice at 10–12 wk of age were also about double those in control mice, whereas the number of splenic $CD8^+$ T cells did not differ significantly between the two genotypes (Fig. 2C). Moreover, the numbers of $F4/80^+$ macrophages, $Gr\text{-}1^+$ granulocytes, and $TER119^+$ erythroblasts in the spleen of Shp1 CKO mice were significantly greater than those in control mice (Fig. 2C), suggesting that the splenomegaly of Shp1 CKO mice is attributable to increased numbers of various cell types.

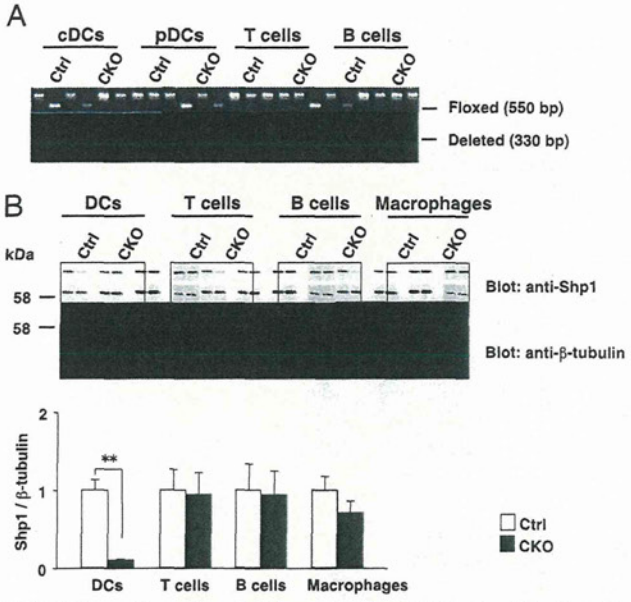

FIGURE 1. Generation of DC-specific Shp1 CKO mice. (**A**) Genomic DNA extracted from cDCs, pDCs, T cells, or B cells sorted from splenocytes of control or Shp1 CKO mice at 12–20 wk of age was subjected to PCR analysis with primers that detect the floxed or deleted alleles of *Ptpn6*. Data are representative of two independent experiments. (**B**) Lysates of DCs, B cells, T cells, or F4/80$^+$ macrophages isolated from the spleen of control or Shp1 CKO mice were subjected to immunoblot analysis with Abs to Shp1 or to β-tubulin (loading control). Blots similar to those shown in the *upper panel* were subjected to densitometric analysis for determination of the ratio of the intensity of the Shp1 band to that of the β-tubulin band (*lower panel*). The quantitative data are expressed relative to the value for control mice and are means ± SE for three mice of each genotype, each of which was examined in an independent experiment. $^{**}p < 0.01$ (Student *t* test). Ctrl, control.

The numbers of both cDCs and pDCs were also markedly increased in the spleen of Shp1 CKO mice at 10–12 wk of age compared with those in the spleen of control mice (Fig. 2D). The cDC population comprises CD4$^+$CD8$^-$ cDCs (CD4$^+$ cDCs), CD4$^-$CD8$^-$ cDCs [double negative (DN) cDCs], and CD4$^-$CD8$^+$ cDCs (CD8$^+$ cDCs) (33, 34). Among these cDC subpopulations, the proportion and the absolute number of DN cDCs in the spleen were markedly increased in Shp1 CKO mice, whereas those of either CD4$^+$ cDCs or CD8$^+$ cDCs were similar for Shp1 CKO and control mice (Fig. 2D). Most CD4$^+$ cDCs and DN cDCs are present in the marginal zone of splenic lymphoid follicles as well as in the marginal zone bridging regions, whereas CD8$^+$ cDCs localize preferentially to the periarteriolar lymphoid sheaths, which are populated mostly by T cells, in the white pulp of the spleen (35). However, immunohistofluorescence analysis revealed that staining for CD11c in the spleen, particularly that in the Thy1.2-positive splenic T cell zones, was greatly increased in Shp1 CKO mice compared with that in the spleen of control mice (Fig. 2E, 2F), suggesting that the distribution of the excess DCs in the spleen of Shp1 CKO mice is disturbed.

In peripheral LNs, the proportion as well as the absolute number of cDCs (but not pDCs) also slightly increased in Shp1 CKO mice at 10–12 wk of age, although such increases were not statistically significant (Supplemental Fig. 2). In contrast, these parameters in the thymus did not differ between Shp1 CKO and control mice at 10–12 wk of age (Supplemental Fig. 2).

Upregulation of DC functions in Shp1 CKO mice

We next examined if the ability of DCs to take up and process Ag might be affected in Shp1 CKO mice. To this end, we incubated purified splenic CD11c$^+$ DCs with DQ-OVA, a self-quenching fluorescently labeled OVA molecule that is degraded to fluorescent peptides after its uptake and intracellular processing (36). We found that neither the uptake nor the processing of DQ-OVA by splenic CD11c$^+$ DCs differed substantially between Shp1 CKO and control mice (Fig. 3A). We next examined the expression of activation markers on CD11c$^+$ DCs under the basal condition. The expression level of CD86 on CD11c$^+$ DCs from the spleen of Shp1 CKO mice at 10–12 wk of age was markedly higher than that for control mice, whereas the expression levels of MHC class II molecules, CD40, and CD80 appeared similar between the two genotypes (Fig. 3B). Moreover, the expression level of CCR7 on splenic CD11c$^+$ DCs of Shp1 CKO mice was substantially higher than that for control mice (Fig. 3B).

We then evaluated the migratory ability of DCs in Shp1 CKO mice. Local application of FITC as a hapten to the skin induces an inflammatory immune response that is studied as a model of contact hypersensitivity (28). It elicits robust migration of DCs in the skin, such as Langerhans cells and dermal DCs, to draining LNs. The total cell number and the number of MHC class II^{high} cells [which represent migratory DCs such as Langerhans cells and dermal DCs from the skin (37, 38)] in the axillary and inguinal LNs did not differ markedly between Shp1 CKO and control mice under the basal condition (data not shown). In contrast, after painting of FITC on the thorax and abdomen, the number of FITC-bearing MHC class II^{high} cells in the LNs of Shp1 CKO mice was significantly increased compared with that apparent for control mice (Fig. 3C), suggesting that the migratory response of skin DCs to FITC painting is upregulated in Shp1 CKO mice.

On activation by pattern recognition receptors such as TLRs, DCs secrete a variety of inflammatory cytokines that are thought to be important for regulation of DC activity and differentiation of effector Th cells (2). We observed that the basal or LPS-induced production of TNF-α, IL-6, IL-1β, and IL-10 by splenic CD11c$^+$ DCs of Shp1 CKO mice was markedly increased compared with that apparent for control mice (Fig. 4A). By contrast, the LPS-induced production of IL-12 (p40) was markedly decreased in CD11c$^+$ DCs from Shp1 CKO mice compared with that apparent for control mice, whereas the basal production of this cytokine did not differ between the two strains (Fig. 4A). In addition, the basal or LPS-stimulated production of IFN-β was also greatly increased in CD11c$^+$ DCs from the spleen of Shp1 CKO mice (Fig. 4A).

To investigate further the molecular mechanism by which Shp1 regulates the LPS-induced production of proinflammatory cytokines, we examined the effects of inhibitors of signaling molecules implicated in this process (39, 40) on the production of IL-6 from splenic DCs of Shp1 CKO mice (Fig. 4B). Treatment with either PDTC or JSH-23, inhibitors of the transcription factor NF-κB (41, 42), markedly decreased IL-6 production from splenic DCs of either Shp1 CKO or control mice in the presence of LPS (Fig. 4B). In addition, treatment with either SB203580 or SP600125, an inhibitor of p38 MAPK or JNK, respectively, also reduced IL-6 production from splenic DCs of either Shp1 CKO or control mice in the presence of LPS (Fig. 4B). In contrast, treatment with wortmannin as an inhibitor of PI3K (Fig. 4B), bisindolylmaleimide I, an inhibitor of protein kinase C, or the Src inhibitor PP2 (data not shown) did not affect the enhanced production of IL-6 by splenic DCs of Shp1 CKO mice. We also examined the abundance of tyrosine-phosphorylated proteins in CD11c$^+$ DCs from the spleen of Shp1 CKO mice. The extent of tyrosine phosphorylation of proteins with molecular masses of ~100 and ~70 kDa was markedly increased in CD11c$^+$ DCs from the spleen of Shp1 CKO mice under either basal or LPS-stimulated conditions compared with that apparent for control mice (Fig. 4C).

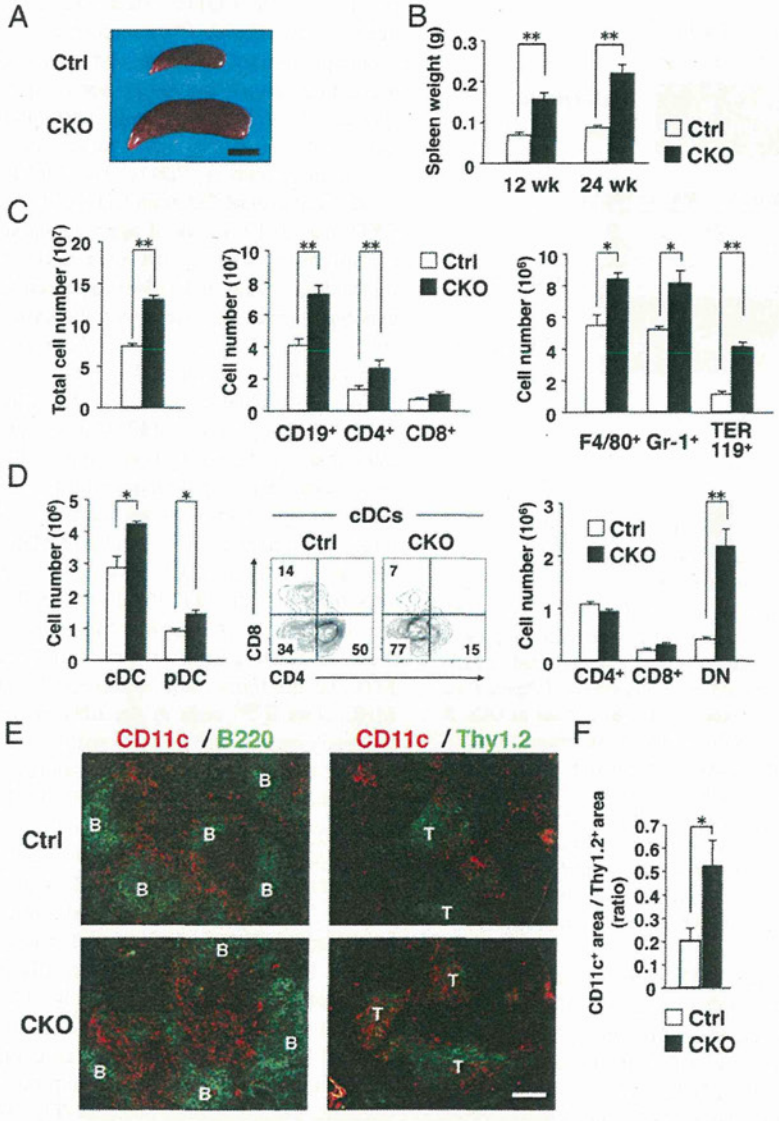

FIGURE 2. Importance of Shp1 in DCs for homeostatic regulation of hematopoietic cells in the spleen. (**A**) Appearance of the spleen of control or Shp1 CKO mice at 26 wk of age. Scale bar, 5 mm. (**B**) Weight of the spleen of control or Shp1 CKO mice at 12 or 24 wk of age. Data are means ± SE from six (12 wk) or five (24 wk) mice per group. $^{**}p < 0.01$ (Student *t* test). (**C**) The total number of splenocytes for control or Shp1 CKO mice at 10–12 wk of age was determined with the use of a Bürker–Türk counting chamber (*left panel*); data are means ± SE for a total of six mice per group analyzed in two independent experiments. The splenocytes were also stained for flow cytometric determination of the absolute numbers of $CD19^+$ B cells, $CD4^+$ T cells, $CD8^+$ T cells, $F4/80^+$ macrophages, $Gr\text{-}1^+$ granulocytes, and $TER119^+$ erythroblasts in PI-negative splenocytes (*middle* and *right panels*); data are means ± SE for three mice per group and are representative of five independent experiments. $^*p < 0.05$, $^{**}p < 0.01$ (Student *t* test). (**D**) Splenocytes isolated from control or Shp1 CKO mice at 10–12 wk of age were stained for CD4, CD8, CD11c, and B220 as well as with PI and were then analyzed by flow cytometry for determination of the absolute numbers of $CD11c^{high}B220^-$ cells (cDCs) and $CD11c^{int}B220^+$ cells (pDCs) (*left panel*), the percentages of $CD4^-CD8^+$ ($CD8^+$ cDCs), $CD4^+CD8^-$ ($CD4^+$ cDCs), and $CD4^-CD8^-$ (DN cDCs) cells among cDCs (*middle panel*), and the absolute numbers of $CD4^+$ cDCs, $CD8^+$ cDCs, and DN cDCs (*right panel*), as indicated. Absolute cell numbers are means ± SE for three mice per group and are representative of five independent experiments. $^*p < 0.05$, $^{**}p < 0.01$ (Student *t* test). (**E**) Frozen sections of the spleen from control or Shp1 CKO mice at 10–12 wk of age were stained with FITC-conjugated Abs to B220 (green, *left panels*) or to Thy1.2 (green, *right panels*) as well as with biotin-conjugated Abs to CD11c and Cy3-conjugated streptavidin (red). Data are representative of three independent experiments. B and T represent B and T cell areas, respectively. Scale bar, 200 μm. (**F**) By the use of ImageJ software, the Thy1.2-positive area (T cell zone) and the CD11c-positive area in the T cell zone were measured. Data are shown as ratios of the CD11c-positive area to the Thy1.2-positive area. Data are means ± SE for 28 (control mice) and 23 (Shp1 CKO mice) follicles from a total of three mice per group examined in three independent experiments. $^*p < 0.05$ (Student *t* test).

High frequency of Th1 cells and increased ability of DCs to promote differentiation of $CD4^+$ T cells into Th1 cells in Shp1 CKO mice

We next examined the effect of Shp1 ablation in $CD11c^+$ DCs on T cell populations in the spleen. The frequency of activated ($CD62L^{low}CD44^{high}$) T cells (43) among either $CD4^+$ or $CD8^+$ T cells was markedly increased in the spleen of Shp1 CKO mice at 20–24 wk of age compared with that for control mice (Fig. 5A), although the frequency of such cells did not differ between the two strains at 10–12 wk of age (data not shown). Moreover, the frequency of IFN-γ–producing $CD4^+$ T cells in the spleen of Shp1 CKO mice at 20–24 wk of age was increased >3-fold compared with that for control mice, whereas the frequency of IL-17– or IL-4–producing $CD4^+$ T cells did not differ between the two genotypes (Fig. 5B). These results indicated that, by 20 wk of age, activation of peripheral T cells and differentiation of $CD4^+$ T cells

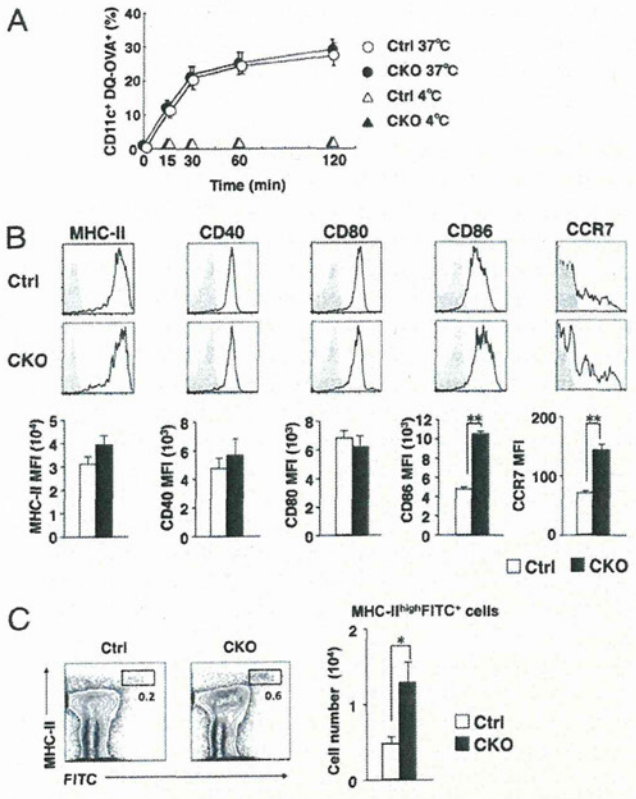

FIGURE 3. Upregulation of DC functions in Shp1 CKO mice. (**A**) Splenic CD11c$^+$ DCs isolated from control or Shp1 CKO mice at 12–16 wk of age were incubated with DQ-OVA (100 ng/ml) for 0–120 min at 37°C or 4°C (negative control), washed, stained with PI, and analyzed by flow cytometry for fluorescent degradation products of DQ-OVA. Data represent the percentage of fluorescence-positive cells among total DCs at each time point; they are means ± SE for three mice per group and are representative of two independent experiments. (**B**) Splenocytes from control or Shp1 CKO mice at 10–12 wk of age were stained for CD11c as well as MHC class II molecules (MHC-II), CD40, CD80, CD86, or CCR7 (open traces), or with isotype control Abs (filled traces), and PI for analysis by flow cytometry. Representative profiles for the expression of MHC class II, CD40, CD80, CD86, or CCR7 on PI-negative CD11c$^+$ cells (*upper panels*) as well as corresponding mean fluorescence intensity (MFI) values (*lower panels*) are shown. MFI data are means ± SE for three mice per group and are representative of three independent experiments. $^{**}p < 0.01$ (Student *t* test). (**C**) Control or Shp1 CKO mice at 12–16 wk of age were painted on the shaved thorax and abdomen with 200 μl 1% FITC. After 24 h, cells were prepared from inguinal and axillary LNs, stained with Abs to MHC class II and with PI, and then analyzed by flow cytometry. The percentage of MHC class II^{high}FITC$^+$ cells among all viable cells on each plot is indicated (*left panel*). The absolute numbers of MHC class II^{high} FITC$^+$ cells were also determined (*right panel*); data are means ± SE for a total of four mice per group examined in two independent experiments. $^*p < 0.05$ (Student *t* test).

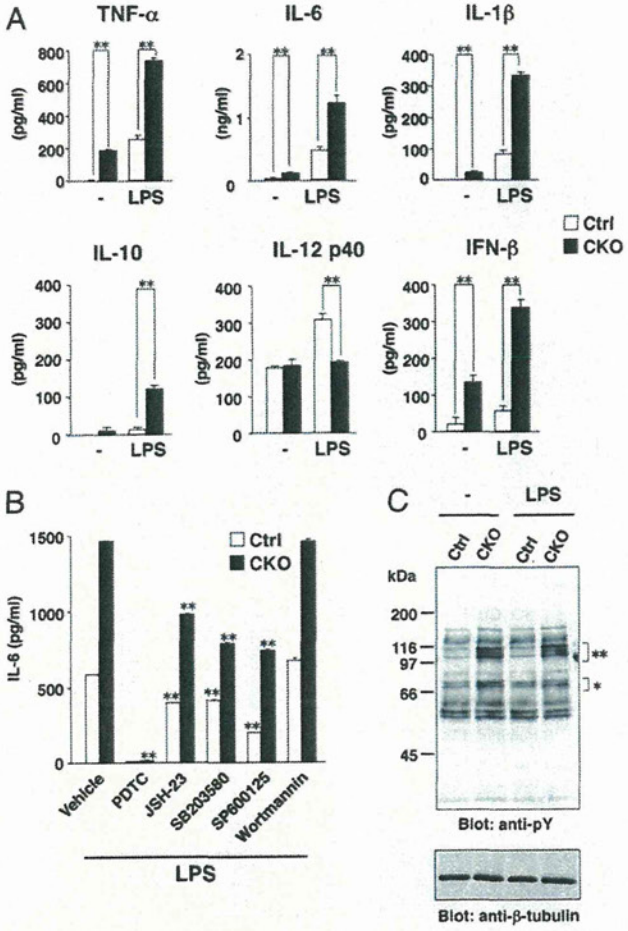

FIGURE 4. Upregulation of proinflammatory cytokine production by DCs from Shp1 CKO mice. (**A**) Splenic CD11c$^+$ DCs from control or Shp1 CKO mice at 12–16 wk of age were cultured in the absence or presence of LPS (1 μg/ml) for 24 h, after which the concentrations of TNF-α, IL-6, IL-1β, IL-10, IL-12 (p40), and IFN-β in culture supernatants were determined. Data are means ± SE of triplicate determinations and are representative of three independent experiments. $^{**}p < 0.01$ (Student *t* test). (**B**) Splenic CD11c$^+$ DCs from control or Shp1 CKO mice were exposed to LPS (1 μg/ml) for 24 h in the absence (vehicle) or presence of the indicated inhibitors of signaling molecules [PDTC (100 μM), JSH-23 (10 μM), SB203580 (10 μM), SP600125 (10 μM), and wortmannin (100 nM)], after which the concentration of IL-6 in culture supernatants was determined. Data are means ± SE of triplicates and are representative of three independent experiments. $^{**}p < 0.01$ (versus the corresponding value for vehicle only in either Shp1 CKO mice or control; Student *t* test). (**C**) Splenic CD11c$^+$ DCs from control or Shp1 CKO mice were exposed to LPS (1 μg/ml) for 15 min, after which cell lysates were prepared and subjected to immunoblot analysis with Abs to phosphotyrosine (pY) or to β-tubulin. Data are representative of three independent experiments. ** and * indicate proteins of ~100 and ~70 kDa, respectively, whose level of tyrosine phosphorylation was increased in CKO mice compared with that in control mice.

toward the Th1 effector lineage were enhanced in Shp1 CKO mice.

We therefore next examined the ability of CD11c$^+$ DCs to promote the Ag-specific proliferation of, as well as the production of IFN-γ by, CD4$^+$ T cells. The proliferation of OVA-specific CD4$^+$ T cells from OT-II mice (25) was increased to a markedly greater extent on culture with OVA-pulsed CD11c$^+$ DCs prepared from Shp1 CKO mice compared with those prepared from control mice (Fig. 5C). Furthermore, the production of IFN-γ, but not that of IL-17, in such cultures was greater with OVA-pulsed CD11c$^+$ DCs of Shp1 CKO mice than with those from control mice (Fig. 5C). These results suggested that the ability of CD11c$^+$ DCs of Shp1 CKO mice to prime and to promote the differentiation of Ag-specific CD4$^+$ T cells to Th1 cells is enhanced compared with that of such cells of control mice.

We also found that the frequency of Foxp3$^+$ Tregs among total CD4$^+$ cells in the spleen was markedly increased for Shp1 CKO mice compared with control mice (Fig. 5D). We also examined the T cell populations in the thymus of Shp1 CKO mice, given that DCs are thought to regulate clonal deletion of self-reactive T cells

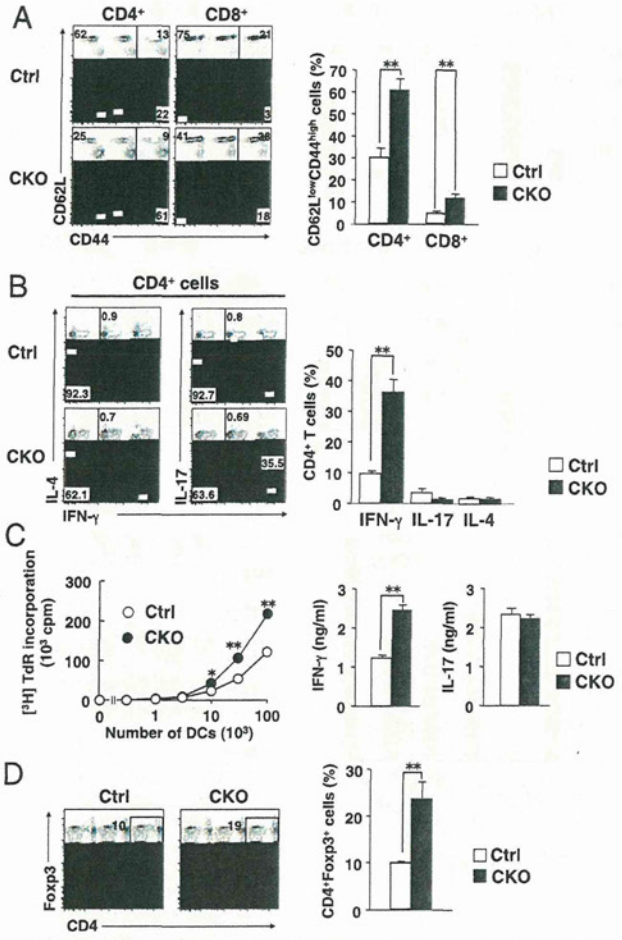

FIGURE 5. High frequency of Th1 cells and increased ability of DCs to promote differentiation of $CD4^+$ T cells into Th1 cells in Shp1 CKO mice. (**A**) Splenocytes from control or Shp1 CKO mice at 20–24 wk of age were stained for CD62L, CD8, CD44, and CD4 as well as with PI, and the expression of CD44 and CD62L on viable $CD4^+$ or $CD8^+$ cells was analyzed by flow cytometry. The percentage of activated ($CD62L^{low}$ $CD44^{high}$) $CD4^+$ or $CD8^+$ cells among all viable $CD4^+$ or $CD8^+$ cells was determined; data are means ± SE for a total of five mice per group examined in three independent experiments. $^{**}p < 0.01$ (Student *t* test). (**B**) Splenocytes from control or Shp1 CKO mice at 20–24 wk of age were stimulated with PMA (100 ng/ml) and ionomycin (1 μg/ml) for 4 h in the presence of GolgiPlug. The cells were then stained for CD4, fixed, permeabilized, and stained again for IFN-γ and either IL-4 or IL-17A. The intracellular expression of IFN-γ, IL-17, or IL-4 in $CD4^+$ cells was then analyzed by flow cytometry. The percentage of cells that express IFN-γ, IL-17, or IL-4 among total $CD4^+$ cells was determined; data are means ± SE for a total of five mice per group examined in three independent experiments. $^{**}p < 0.01$ (Student *t* test). (**C**) Control or Shp1 CKO mice at 12–16 wk of age were injected intravenously with 3 mg OVA. After 12 h, splenic $CD11c^+$ DCs were isolated from the mice and were cultured for 72 h at various densities with $CD4^+$ T cells (1×10^5) from OT-II mice. Cell proliferation (*left panel*) as well as the concentrations of IFN-γ and IL-17 in culture supernatants (*right panels*) were then determined. Data are means ± SE of triplicate determinations and are representative of three separate experiments. $^{*}p < 0.05$, $^{**}p < 0.01$ (versus the corresponding value for control mice or for the indicated comparison; Student *t* test). (**D**) Splenocytes from control or Shp1 CKO mice at 20–24 wk of age were stained for CD4, fixed, permeabilized, and stained again for Foxp3. The intracellular expression of Foxp3 in $CD4^+$ cells was then analyzed by flow cytometry. The percentage of $CD4^+Foxp3^+$ cells among total $CD4^+$ splenocytes was determined; data are means ± SE for a total of five mice per group examined in three independent experiments. $^{**}p <$ 0.01 (Student *t* test).

in the thymus (44). The frequency of either single-positive (CD4 or CD8), double-positive, or double-negative (DN1 to DN4) thymocytes, however, did not differ between Shp1 CKO and control mice (Supplemental Fig. 3).

Increased number of B-1a cells and elevation of serum concentrations of IgM and IgG2a in Shp1 CKO mice

Given that the frequency of B cells in the spleen of Shp1 CKO mice was about twice that for control mice (Fig. 2C), we examined the effect of DC-specific Shp1 deficiency on B cell subpopulations in the spleen. The frequency of marginal-zone B cells ($CD21^{high}$ $CD23^{low}$) (45) among matured B cells ($B220^+AA4.1^-$) (45) was decreased in the spleen of Shp1 CKO mice at 10–12 wk of age compared with that for control mice (Fig. 6A), whereas the frequency of follicular B cells ($CD21^{high}CD23^{high}$) (45) did not differ between the two strains. The frequency of either T1 ($CD21^{high}$ $CD23^{high}$) or T2 ($CD21^{low}CD23^{low}$) B cells among immature B cells ($B220^+AA4.1^+$) did not differ between the two genotypes (Fig. 6A). The population of activated B cells ($B220^+CD69^+$) (46) among $B220^+$ B cells was markedly increased compared with that for control mice at 10–12 wk of age (Fig. 6B), suggesting that Shp1 deficiency in DCs results in activation of B cells in the spleen.

Mature splenic B cells consist mostly of two subtypes, B-1a and B-2 cells (47). B-1a cells constitute a relatively small subpopulation of splenic B cells defined by the expression of CD5, and they spontaneously secrete IgM. The number of B-1a cells is markedly increased in the spleen of *motheaten* mice (20). The proportion of $CD19^+CD5^+$ (B-1a) cells among splenocytes of Shp1 CKO mice was markedly increased compared with that for control mice at 10–12 wk of age (Fig. 6C), suggesting that Shp1 deficiency in DCs affects development of B-1a cells in the spleen. To examine further the effect of DC-specific Shp1 deficiency on B cell function, we measured the concentrations of Ig isotypes in serum. The serum concentrations of IgM and IgG2a were markedly increased in Shp1 CKO mice at 20–24 wk of age compared with those apparent for control mice, whereas the levels of IgA, IgG1, IgG2b, and IgG3 did not differ between the two strains (Fig. 6D).

DCs are an important source of BAFF and APRIL, both of which are thought to promote B cell survival and plasmablast differentiation (48). However, the amounts of BAFF and APRIL mRNAs in splenic $CD11c^+$ DCs did not differ between control and Shp1 CKO mice (Supplemental Fig. 4).

Shp1 CKO mice develop autoimmunity

Motheaten mice develop systemic autoimmune disease such as glomerulonephritis and interstitial pneumonitis, with accompanying hypergammaglobulinemia, high titers of autoantibodies, and immune complex deposition (20) We therefore next investigated whether Shp1 CKO mice similarly develop autoimmune disease. H&E staining revealed massive leukocyte accumulation and hypercellularity in renal glomeruli as well as prominent leukocyte infiltration at lung alveoli of Shp1 CKO mice at 36–40 wk of age (Fig. 7A–C), suggesting that aged Shp1 CKO mice develop glomerulonephritis as well as interstitial pneumonitis. In addition, the CKO mice at 20–24 wk of age manifested a slightly increased level of leukocyte accumulation at lung alveoli (data not shown). We also found that staining for IgG and C3, which reflects immune complex deposition, was markedly increased in renal glomeruli of aged Shp1 CKO mice (Fig. 7D, 7E). Consistent with the histological data, aged Shp1 CKO mice manifested impairment of the renal function, as the levels of blood urea nitrogen and of

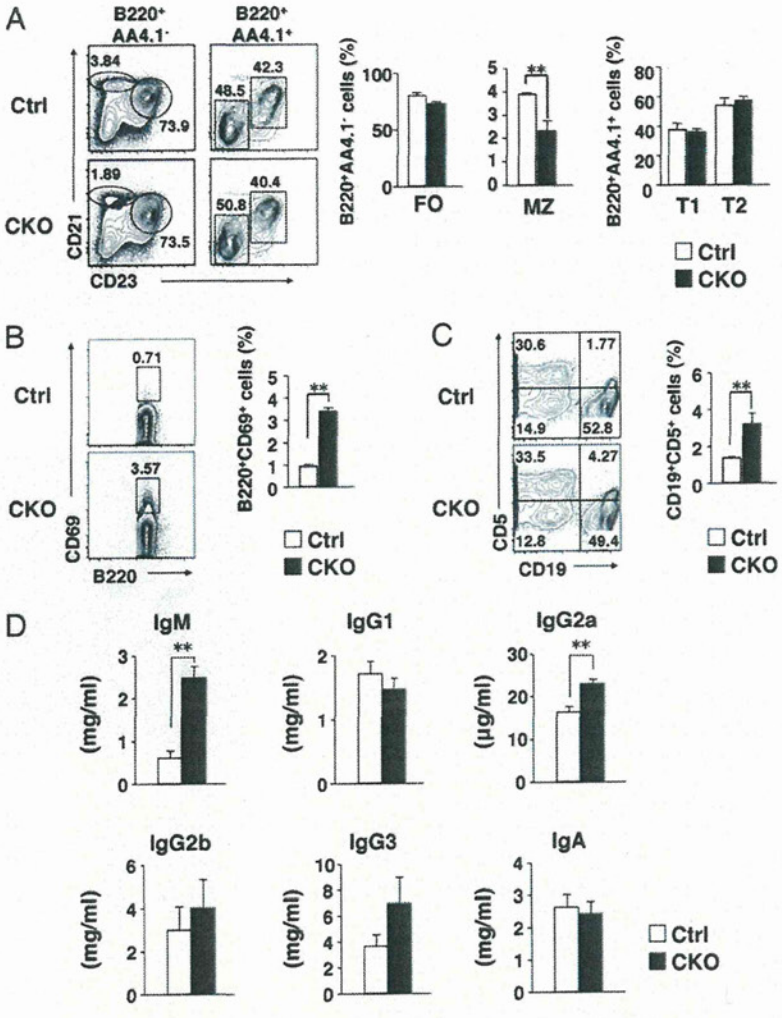

FIGURE 6. Analysis of B cell populations and serum Ig concentrations in Shp1 CKO mice. (**A**) Splenocytes from control or Shp1 CKO mice at 10–12 wk of age were stained for B220, AA4.1, CD21, and CD23 as well as with PI for analysis of follicular (FO) B ($CD21^{high}CD23^{high}$) and marginal-zone (MZ) B ($CD21^{high}CD23^{low}$) cells within the $B220^+AA4.1^-$-gated mature B cell population and of transitional T1 ($CD21^{high}CD23^{high}$) and T2 ($CD21^{low}CD23^{low}$) B cells within the $B220^+AA4.1^+$-gated immature B cells by flow cytometry (*left panel*). The percentage of MZ B cells or FO B cells among viable $B220^+AA4.1^-$ cells and that of T1 or T2 B cells among viable $B220^+AA4.1^+$ cells were determined (*middle* and *right panels*); data are means ± SE for three mice per group and are representative of two independent experiments. $^{**}p < 0.01$ (Student *t* test). (**B**) Splenocytes from control or Shp1 CKO mice at 10–12 wk of age were stained for B220 and CD69 as well as with PI for analysis of B220 and CD69 expression in all viable cells by flow cytometry. The percentage of activated B ($B220^+CD69^+$) cells among viable $B220^+$ cells was determined; data are means ± SE for three mice per group and are representative of two independent experiments. $^{**}p < 0.01$ (Student *t* test). (**C**) Splenocytes from control or Shp1 CKO mice at 10–12 wk of age were stained for CD19 and CD5 as well as with PI for analysis of CD19 and CD5 expression in viable cells by flow cytometry. The percentage of B-1a ($CD19^+CD5^+$) cells among all viable cells was determined; data are means ± SE for three mice per group and are representative of three independent experiments. $^{**}p < 0.01$ (Student *t* test). (**D**) Serum concentrations of IgM, IgG1, IgG2a, IgG2b, IgG3, and IgA in control or Shp1 CKO mice at 20–24 wk of age. Data are means ± SE for six mice per group and are representative of two independent experiments. $^{**}p < 0.01$ (Student *t* test).

serum creatinine in CKO mice were significantly higher than those of control mice (Fig. 7F). Moreover, the CKO mice had significantly higher serum titer of ANA as well as of IgG Abs to dsDNA compared with age-matched control mice (Fig. 7G).

Discussion

We have shown that Shp1 in $CD11c^+$ DCs is important for homeostatic regulation of both cDCs and pDCs in the spleen. The number of DN cDCs was markedly increased in the spleen of Shp1 CKO mice, whereas that of $CD4^+$ cDCs or $CD8^+$ cDCs was similar for Shp1 CKO and control mice. We also found that the incorporation rate of BrdU into splenic cDCs in the CKO mice was higher than that apparent with control mice (data not shown), suggesting that the proliferation and differentiation of cDCs likely increase in Shp1 CKO mice. All three subtypes of cDCs are thought to arise from the immediate precursors of cDCs, defined as lineage-negative $CD11c^+$MHC class II^-FLT3^+ cells (49). It is thus likely that Shp1 is required in a cell-autonomous manner for negative regulation of the development of cDCs, in particular that of DN cDCs, in the spleen. In contrast, an increase in the number of cDCs was not observed in either peripheral LNs or the thymus of Shp1 CKO mice, suggesting that the regulation of cDC homeostasis in the spleen differs from that in LNs and the thymus.

We have also shown that Shp1 is a negative regulator of multiple DC functions that are thought to be important for the promotion by DCs of the differentiation of naive T cells into Th cells. First, the migratory response of DCs to FITC painting was upregulated in Shp1 CKO mice, suggesting that Shp1 negatively regulates the ability of DCs to migrate to draining LNs after they have captured exogenous Ags. In addition, the expression level of CCR7 on $CD11c^+$ DCs was also upregulated in Shp1 CKO mice. Given that CCR7 is a receptor for CCL19 and CCL21, both of which promote DC migration (50), it is likely that Shp1 inhibits DC migration through downregulation of CCR7 expression. Second, expression of CD86, a costimulatory molecule that is important in the priming of naive T cells for their differentiation into Th cells, was also increased in $CD11c^+$ DCs of Shp1 CKO mice. Third, the LPS-induced production of proinflammatory cytokines such as TNF-α, IL-6, and IL-1β, which are implicated in the regulation of DC activity and of the differentiation of effector Th cells (2), was markedly increased in $CD11c^+$ DCs of Shp1 CKO mice.

Consistent with such enhanced activities of DCs in Shp1 CKO mice, the frequency of activated T cells, as well as that of IFN-γ–producing $CD4^+$ T cells, was increased in the spleen of the mutant animals. In contrast, the frequency of IL-17– or IL-4–producing $CD4^+$ T cells in the spleen was unaffected in Shp1 CKO mice. Moreover, the ability of $CD11c^+$ DCs from the spleen of Shp1 CKO mice to prime and induce Th1 (but not Th17) differentiation of OVA-specific $CD4^+$ T cells was enhanced. Shp1 in $CD11c^+$ DCs is thus important specifically for negative regulation of priming and Th1 differentiation of $CD4^+$ T cells by DCs. LPS-stimulated production of IL-12, a cytokine that is thought to be required for induction of Th1 cells from naive $CD4^+$ T cells, was markedly decreased in $CD11c^+$ DCs from Shp1 CKO mice, in-

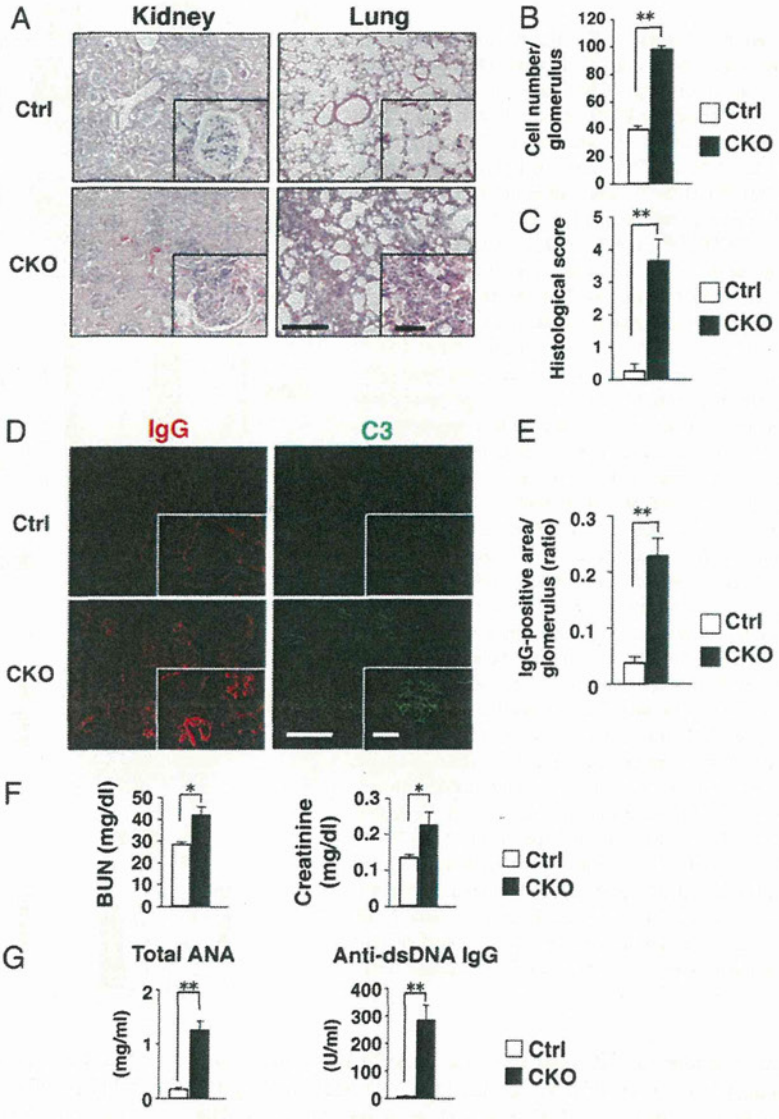

FIGURE 7. Development of autoimmunity in Shp1 CKO mice. (**A**) Paraffin-embedded sections of the kidney (*left panels*) and lung (*right panels*) from control or Shp1 CKO mice at 36–40 wk of age were stained with H&E. Images are representative of those from nine mice per group. *Insets* show higher magnification images of glomerulus and alveolar septa. Scale bars, 200 μm and 50 μm (*insets*). (**B**) For quantitative assessment of glomerular pathology, glomerular cellularity was examined by counting the number of cells with nuclei per each glomerulus. Twenty glomeruli of a similar size were examined for each animal. Data are means ± SE for a total of four mice per group. (**C**) Histological changes of the lung were also determined quantitatively by scoring of the following three categories (58): 1) interstitial infiltrates of lymphocytes and macrophages 2), perivascular infiltrates of lymphocytes and macrophages, and 3) expansion of BALT. Each category was scored as follows: 0, none; 1, mild; 2, moderate to severe. The sum of these scores thus represents the severity of inflammation with a maximum possible of 6. Data are means ± SE for a total of nine mice per group. $^{**}p < 0.01$ (Student *t* test). (**D**) Frozen sections of the kidney from control or Shp1 CKO mice at 36–40 wk of age were subjected to immunohistofluorescence analysis of IgG (red) or C3 (green). *Insets* show higher magnification images of glomerulus. Scale bars, 200 μm and 50 μm (*insets*). Images are representative of those from nine (IgG) or three (C3) mice of each genotype. (**E**) A ratio of the IgG-positive area to that for a single glomerulus was determined by the use of ImageJ software. Data are means ± SE for 11 (control) and 15 (Shp1 CKO) glomeruli from total of three mice per group examined in three independent experiments. $^{**}p < 0.01$ (Student *t* test). (**F**) Levels of blood urea nitrogen (BUN) and of serum creatinine in control or Shp1 CKO mice at 36–40 wk of age were determined. Data are means ± SE for eight mice per group. $^{*}p < 0.05$ (Student *t* test). (**G**) Serum titers of total ANA and anti-dsDNA IgG in control or Shp1 CKO mice at 36–40 wk of age. Data are means ± SE for nine mice per group. $^{**}p < 0.01$ (Student *t* test).

dicating that in contrast to other proinflammatory cytokines, the LPS-dependent production of IL-12 by CD11c$^+$ DCs is positively regulated by Shp1. This finding is consistent with the recent observation that bone marrow-derived macrophages prepared from *me^v/me^v* mice manifested marked impairment of LPS-induced IL-12 production (51). In contrast, Ramachandran et al. (22) reported that inhibition of Shp1 activity by a specific inhibitor of Shp1 increased the LPS-driven IL-12 production in bone marrow-derived DCs. Such difference may be attributable to that we or Zhou et al. (51) used isolated splenic DCs from Shp1 CKO mice or bone marrow-derived macrophages from *me^v/me^v* mice, respectively, whereas Ramachandran et al. (22) used bone marrow-derived DCs from wild-type mice. Thus, the reduced IL-12 production in Shp1 CKO or *me^v/me^v* mice may be, in part, an epiphenomenon due to disruption of splenic homeostasis in these mice. By contrast, expression of Delta 4 Notch-like ligand (52) or that of CD70 (53) on DCs is important for Th1 differentiation in a manner independent of IL-12. Indeed, we found that expression of CD70 on CD11c$^+$ DCs was markedly increased in the spleen of Shp1 CKO mice compared with control mice (data not shown). Thus, increased expression of CD70 on DCs might contribute to specific increase of Th1 differentiation in Shp1 CKO mice.

The molecular mechanism by which Shp1 negatively regulates the LPS-induced production of proinflammatory cytokines by CD11c$^+$ DCs remains largely unknown. However, we found that the enhancement of LPS-stimulated proinflammatory cytokine production apparent in DCs from Shp1 CKO mice was prevented by inhibitors of NF-κB activity, suggesting that Shp1 suppresses NF-κB–dependent signaling. In addition, Shp1 likely suppresses p38 MAPK- or JNK-dependent pathways in DCs. Moreover, the extent of tyrosine phosphorylation of proteins of ~70 and ~100 kDa was indeed increased in CD11c$^+$ DCs from the spleen of Shp1 CKO mice compared with that apparent for control mice. Characterization of these proteins as targets of the PTP activity of Shp1 in DCs may provide further insight into the molecular mechanism by which Shp1 negatively regulates DC functions.

DCs are also thought to play an important role in regulation of peripheral T cell tolerance through the production of IL-10 (3) as well as induction of Tregs (5, 6). However, the production of IL-10 in response to LPS was enhanced in isolated DCs from Shp1 CKO mice. In addition, the frequency of Tregs in the spleen was markedly increased in these animals. These results thus indicate that Shp1 in DCs is also a negative regulator of IL-10 production by DCs as well as of Treg homeostasis in the spleen. They further

suggest that peripheral T cell tolerance is not likely impaired in Shp1 CKO mice.

Shp1 CKO mice manifested increases both in the number of $CD5^+CD19^+$ (B-1a) cells in the spleen as well as in the concentrations of IgM and IgG2a in serum. Given that ~80% of IgM in serum is thought to be derived from B-1a cells (47), the increase in the serum level of IgM in Shp1 CKO mice is likely attributable in large part to the increase in the number of splenic B-1a cells. Shp1 in DCs is thus important for regulation of the homeostasis of B-1a cells in the spleen, although the molecular mechanism underlying such regulation remains unknown. In contrast, B cells are thought to secrete IgG2a in response to IFN-γ (54). It is therefore likely that the increase in the serum concentration of IgG2a in Shp1 CKO mice is attributable to the increase in the number of activated Th1 cells.

Shp1 CKO mice spontaneously developed systemic autoimmunity including glomerulonephritis and interstitial pneumonitis, with the former being associated with immune complex deposition in glomeruli. In addition, Shp1 CKO mice had markedly increased serum titers of autoantibodies such as ANA and anti-dsDNA. Defective regulation of either T cell immune responses or peripheral T cell tolerance by DCs is thought to give rise to autoimmunity (4, 10, 55). Our current results thus indicate that Shp1 in DCs plays an important role in protection against development of systemic autoimmunity, likely by limiting the development of Th1 cells. Moreover, development of SLE is thought to be attributable to activation of DCs in response to an excess of IFN-αβ (56). Given that DCs of Shp1 CKO mice manifested increased production of IFN-β in response to LPS, Shp1 also appears to be important for negative regulation of type I IFN production by DCs and consequent protection against SLE-like autoimmunity. The observation that me^v/me^v mice on the $Rag1^{-/-}$ background, which lack both T and B cells, also develop autoimmunity suggests that the loss of Shp1 in myeloid cells is important for development of autoimmunity in these mice (57).

In summary, we have shown that Shp1 negatively regulates various functions of DCs, in particular the promotion of Th1 cell differentiation, and that it thereby protects against autoimmunity. Development of an approach to activate Shp1 specifically in DCs may provide the basis for a potential new therapy for various autoimmune diseases.

Acknowledgments

We thank B.G. Neel and L.I. Pao for providing $Ptpn6^{fl/fl}$ mice, K. Okumura for the mAb to CD16/32, T. Hirano for OT-II mice, and H. Kobayashi, Y. Niwayama-Kusakari, E. Urano, and R. Koitabashi for technical assistance.

Disclosures

The authors have no financial conflicts of interest.

References

1. Steinman, R. M., and J. Banchereau. 2007. Taking dendritic cells into medicine. *Nature* 449: 419–426.
2. Coquerelle, C., and M. Moser. 2010. DC subsets in positive and negative regulation of immunity. *Immunol. Rev.* 234: 317–334.
3. Akbari, O., R. H. DeKruyff, and D. T. Umetsu. 2001. Pulmonary dendritic cells producing IL-10 mediate tolerance induced by respiratory exposure to antigen. *Nat. Immunol.* 2: 725–731.
4. Travis, M. A., B. Reizis, A. C. Melton, E. Masteller, Q. Tang, J. M. Proctor, Y. Wang, X. Bernstein, X. Huang, L. F. Reichardt, et al. 2007. Loss of integrin $\alpha(v)\beta_8$ on dendritic cells causes autoimmunity and colitis in mice. *Nature* 449: 361–365.
5. Mahnke, K., Y. Qian, J. Knop, and A. H. Enk. 2003. Induction of $CD4^+/CD25^+$ regulatory T cells by targeting of antigens to immature dendritic cells. *Blood* 101: 4862–4869.
6. Luo, X., K. V. Tarbell, H. Yang, K. Pothoven, S. L. Bailey, R. Ding, R. M. Steinman, and M. Suthanthiran. 2007. Dendritic cells with TGF-β1 differentiate naive $CD4^+CD25^-$ T cells into islet-protective $Foxp3^+$ regulatory T cells. *Proc. Natl. Acad. Sci. USA* 104: 2821–2826.
7. Hawiger, D., K. Inaba, Y. Dorsett, M. Guo, K. Mahnke, M. Rivera, J. V. Ravetch, R. M. Steinman, and M. C. Nussenzweig. 2001. Dendritic cells induce peripheral T cell unresponsiveness under steady state conditions in vivo. *J. Exp. Med.* 194: 769–779.
8. Probst, H. C., K. McCoy, T. Okazaki, T. Honjo, and M. van den Broek. 2005. Resting dendritic cells induce peripheral $CD8^+$ T cell tolerance through PD-1 and CTLA-4. *Nat. Immunol.* 6: 280–286.
9. Teichmann, L. L., M. L. Ols, M. Kashgarian, B. Reizis, D. H. Kaplan, and M. J. Shlomchik. 2010. Dendritic cells in lupus are not required for activation of T and B cells but promote their expansion, resulting in tissue damage. *Immunity* 33: 967–978.
10. Ohnmacht, C., A. Pullner, S. B. King, I. Drexler, S. Meier, T. Brocker, and D. Voehringer. 2009. Constitutive ablation of dendritic cells breaks self-tolerance of CD4 T cells and results in spontaneous fatal autoimmunity. *J. Exp. Med.* 206: 549–559.
11. Neel, B. G., H. Gu, and L. Pao. 2003. The 'Shp'ing news: SH2 domain-containing tyrosine phosphatases in cell signaling. *Trends Biochem. Sci.* 28: 284–293.
12. Pao, L. I., K. Badour, K. A. Siminovitch, and B. G. Neel. 2007. Nonreceptor protein-tyrosine phosphatases in immune cell signaling. *Annu. Rev. Immunol.* 25: 473–523.
13. Klingmüller, U., U. Lorenz, L. C. Cantley, B. G. Neel, and H. F. Lodish. 1995. Specific recruitment of SH-PTP1 to the erythropoietin receptor causes inactivation of JAK2 and termination of proliferative signals. *Cell* 80: 729–738.
14. Maeda, A., M. Kurosaki, M. Ono, T. Takai, and T. Kurosaki. 1998. Requirement of SH2-containing protein tyrosine phosphatases SHP-1 and SHP-2 for paired immunoglobulin-like receptor B (PIR-B)-mediated inhibitory signal. *J. Exp. Med.* 187: 1355–1360.
15. Matozaki, T., Y. Murata, H. Okazawa, and H. Ohnishi. 2009. Functions and molecular mechanisms of the CD47-SIRPalpha signalling pathway. *Trends Cell Biol.* 19: 72–80.
16. Shultz, L. D., P. A. Schweitzer, T. V. Rajan, T. Yi, J. N. Ihle, R. J. Matthews, M. L. Thomas, and D. R. Beier. 1993. Mutations at the murine motheaten locus are within the hematopoietic cell protein-tyrosine phosphatase (Hcph) gene. *Cell* 73: 1445–1454.
17. Tsui, H. W., K. A. Siminovitch, L. de Souza, and F. W. Tsui. 1993. Motheaten and viable motheaten mice have mutations in the haematopoietic cell phosphatase gene. *Nat. Genet.* 4: 124–129.
18. Green, M. C., and L. D. Shultz. 1975. Motheaten, an immunodeficient mutant of the mouse. I. Genetics and pathology. *J. Hered.* 66: 250–258.
19. Shultz, L. D., D. R. Coman, C. L. Bailey, W. G. Beamer, and C. L. Sidman. 1984. "Viable motheaten," a new allele at the motheaten locus. I. Pathology. *Am. J. Pathol.* 116: 179–192.
20. Shultz, L. D. 1988. Pleiotropic effects of deleterious alleles at the "motheaten" locus. *Curr. Top. Microbiol. Immunol.* 137: 216–222.
21. Nakayama, K., K. Takahashi, L. D. Shultz, K. Miyakawa, and K. Tomita. 1997. Abnormal development and differentiation of macrophages and dendritic cells in viable motheaten mutant mice deficient in haematopoietic cell phosphatase. *Int. J. Exp. Pathol.* 78: 245–257.
22. Ramachandran, I. R., W. Song, N. Lapteva, M. Seethammagari, K. M. Slawin, D. M. Spencer, and J. M. Levitt. 2011. The phosphatase SRC homology region 2 domain-containing phosphatase-1 is an intrinsic central regulator of dendritic cell function. *J. Immunol.* 186: 3934–3945.
23. Caton, M. L., M. R. Smith-Raska, and B. Reizis. 2007. Notch-RBP-J signaling controls the homeostasis of $CD8^-$ dendritic cells in the spleen. *J. Exp. Med.* 204: 1653–1664.
24. Pao, L. I., K. P. Lam, J. M. Henderson, J. L. Kutok, M. Alimzhanov, L. Nitschke, M. L. Thomas, B. G. Neel, and K. Rajewsky. 2007. B cell-specific deletion of protein-tyrosine phosphatase Shp1 promotes B-1a cell development and causes systemic autoimmunity. *Immunity* 27: 35–48.
25. Barnden, M. J., J. Allison, W. R. Heath, and F. R. Carbone. 1998. Defective TCR expression in transgenic mice constructed using cDNA-based α- and β-chain genes under the control of heterologous regulatory elements. *Immunol. Cell Biol.* 76: 34–40.
26. Tomizawa, T., Y. Kaneko, Y. Kaneko, Y. Saito, H. Ohnishi, J. Okajo, C. Okuzawa, T. Ishikawa-Sekigami, Y. Murata, H. Okazawa, et al. 2007. Resistance to experimental autoimmune encephalomyelitis and impaired T cell priming by dendritic cells in Src homology 2 domain-containing protein tyrosine phosphatase substrate-1 mutant mice. *J. Immunol.* 179: 869–877.
27. Saito, Y., H. Iwamura, T. Kaneko, H. Ohnishi, Y. Murata, H. Okazawa, Y. Kanazawa, M. Sato-Hashimoto, H. Kobayashi, P. A. Oldenborg, et al. 2010. Regulation by SIRPα of dendritic cell homeostasis in lymphoid tissues. *Blood* 116: 3517–3525.
28. Iwamura, H., Y. Saito, M. Sato-Hashimoto, H. Ohnishi, Y. Murata, H. Okazawa, Y. Kanazawa, T. Kaneko, S. Kusakari, T. Kotani, et al. 2011. Essential roles of SIRPα in homeostatic regulation of skin dendritic cells. *Immunol. Lett.* 135: 100–107.
29. Kanazawa, Y., Y. Saito, Y. Supriatna, H. Tezuka, T. Kotani, Y. Murata, H. Okazawa, H. Ohnishi, Y. Kinouchi, Y. Nojima, et al. 2010. Role of SIRPα in regulation of mucosal immunity in the intestine. *Genes Cells* 15: 1189–1200.
30. Shortman, K., and S. H. Naik. 2007. Steady-state and inflammatory dendritic-cell development. *Nat. Rev. Immunol.* 7: 19–30.
31. Hou, B., B. Reizis, and A. L. DeFranco. 2008. Toll-like receptors activate innate and adaptive immunity by using dendritic cell-intrinsic and -extrinsic mechanisms. *Immunity* 29: 272–282.

32. Melillo, J. A., L. Song, G. Bhagat, A. B. Blazquez, C. R. Plumlee, C. Lee, C. Berin, B. Reizis, and C. Schindler. 2010. Dendritic cell (DC)-specific targeting reveals Stat3 as a negative regulator of DC function. *J. Immunol.* 184: 2638–2645.
33. Vremec, D., J. Pooley, H. Hochrein, L. Wu, and K. Shortman. 2000. CD4 and CD8 expression by dendritic cell subtypes in mouse thymus and spleen. *J. Immunol.* 164: 2978–2986.
34. Wu, L., and Y. J. Liu. 2007. Development of dendritic-cell lineages. *Immunity* 26: 741–750.
35. Leenen, P. J., K. Radosević, J. S. Voerman, B. Salomon, N. van Rooijen, D. Klatzmann, and W. van Ewijk. 1998. Heterogeneity of mouse spleen dendritic cells: in vivo phagocytic activity, expression of macrophage markers, and subpopulation turnover. *J. Immunol.* 160: 2166–2173.
36. Zietara, N., M. Łyszkiewicz, N. Gekara, J. Puchałka, V. A. Dos Santos, C. R. Hunt, T. K. Pandita, S. Lienenklaus, and S. Weiss. 2009. Absence of IFN-β impairs antigen presentation capacity of splenic dendritic cells via down-regulation of heat shock protein 70. *J. Immunol.* 183: 1099–1109.
37. Merad, M., F. Ginhoux, and M. Collin. 2008. Origin, homeostasis and function of Langerhans cells and other langerin-expressing dendritic cells. *Nat. Rev. Immunol.* 8: 935–947.
38. Liu, K., and M. C. Nussenzweig. 2010. Origin and development of dendritic cells. *Immunol. Rev.* 234: 45–54.
39. Miyake, A., Y. Murata, H. Okazawa, H. Ikeda, Y. Niwayama, H. Ohnishi, Y. Hirata, and T. Matozaki. 2008. Negative regulation by SHPS-1 of Toll-like receptor-dependent proinflammatory cytokine production in macrophages. *Genes Cells* 13: 209–219.
40. Kawai, T., and S. Akira. 2011. Toll-like receptors and their crosstalk with other innate receptors in infection and immunity. *Immunity* 34: 637–650.
41. Cuzzocrea, S., P. K. Chatterjee, E. Mazzon, L. Dugo, I. Serraino, D. Britti, G. Mazzullo, A. P. Caputi, and C. Thiemermann. 2002. Pyrrolidine dithiocarbamate attenuates the development of acute and chronic inflammation. *Br. J. Pharmacol.* 135: 496–510.
42. Shin, H. M., M. H. Kim, B. H. Kim, S. H. Jung, Y. S. Kim, H. J. Park, J. T. Hong, K. R. Min, and Y. Kim. 2004. Inhibitory action of novel aromatic diamine compound on lipopolysaccharide-induced nuclear translocation of NF-kappaB without affecting IkappaB degradation. *FEBS Lett.* 571: 50–54.
43. Dillon, S. R., C. Sprecher, A. Hammond, J. Bilsborough, M. Rosenfeld-Franklin, S. R. Presnell, H. S. Haugen, M. Maurer, B. Harder, J. Johnston, et al. 2004. Interleukin 31, a cytokine produced by activated T cells, induces dermatitis in mice. *Nat. Immunol.* 5: 752–760.
44. Steinman, R. M., D. Hawiger, and M. C. Nussenzweig. 2003. Tolerogenic dendritic cells. *Annu. Rev. Immunol.* 21: 685–711.
45. Jang, I. K., D. G. Cronshaw, L. K. Xie, G. Fang, J. Zhang, H. Oh, Y. X. Fu, H. Gu, and Y. Zou. 2011. Growth-factor receptor-bound protein-2 (Grb2) signaling in B cells controls lymphoid follicle organization and germinal center reaction. *Proc. Natl. Acad. Sci. USA* 108: 7926–7931.
46. Atencio, S., H. Amano, S. Izui, and B. L. Kotzin. 2004. Separation of the New Zealand Black genetic contribution to lupus from New Zealand Black determined expansions of marginal zone B and B1a cells. *J. Immunol.* 172: 4159–4166.
47. Baumgarth, N. 2011. The double life of a B-1 cell: self-reactivity selects for protective effector functions. *Nat. Rev. Immunol.* 11: 34–46.
48. Mackay, F., P. A. Silveira, and R. Brink. 2007. B cells and the BAFF/APRIL axis: fast-forward on autoimmunity and signaling. *Curr. Opin. Immunol.* 19: 327–336.
49. Liu, K., G. D. Victora, T. A. Schwickert, P. Guermonprez, M. M. Meredith, K. Yao, F. F. Chu, G. J. Randolph, A. Y. Rudensky, and M. Nussenzweig. 2009. In vivo analysis of dendritic cell development and homeostasis. *Science* 324: 392–397.
50. Förster, R., A. Schubel, D. Breitfeld, E. Kremmer, I. Renner-Müller, E. Wolf, and M. Lipp. 1999. CCR7 coordinates the primary immune response by establishing functional microenvironments in secondary lymphoid organs. *Cell* 99: 23–33.
51. Zhou, D., C. A. Collins, P. Wu, and E. J. Brown. 2010. Protein tyrosine phosphatase SHP-1 positively regulates TLR-induced IL-12p40 production in macrophages through inhibition of phosphatidylinositol 3-kinase. *J. Leukoc. Biol.* 87: 845–855.
52. Skokos, D., and M. C. Nussenzweig. 2007. $CD8^-$ DCs induce IL-12-independent Th1 differentiation through Delta 4 Notch-like ligand in response to bacterial LPS. *J. Exp. Med.* 204: 1525–1531.
53. Soares, H., H. Waechter, N. Glaichenhaus, E. Mougneau, H. Yagita, O. Mizenina, D. Dudziak, M. C. Nussenzweig, and R. M. Steinman. 2007. A subset of dendritic cells induces $CD4^+$ T cells to produce IFN-γ by an IL-12-independent but CD70-dependent mechanism in vivo. *J. Exp. Med.* 204: 1095–1106.
54. Snapper, C. M., and W. E. Paul. 1987. Interferon-γ and B cell stimulatory factor-1 reciprocally regulate Ig isotype production. *Science* 236: 944–947.
55. Chen, M., Y. H. Wang, Y. Wang, L. Huang, H. Sandoval, Y. J. Liu, and J. Wang. 2006. Dendritic cell apoptosis in the maintenance of immune tolerance. *Science* 311: 1160–1164.
56. Banchereau, J., V. Pascual, and A. K. Palucka. 2004. Autoimmunity through cytokine-induced dendritic cell activation. *Immunity* 20: 539–550.
57. Yu, C. C., H. W. Tsui, B. Y. Ngan, M. J. Shulman, G. E. Wu, and F. W. Tsui. 1996. B and T cells are not required for the viable motheaten phenotype. *J. Exp. Med.* 183: 371–380.
58. Mankowski, J. L., D. L. Carter, J. P. Spelman, M. L. Nealen, K. R. Maughan, L. M. Kirstein, P. J. Didier, R. J. Adams, M. Murphey-Corb, and M. C. Zink. 1998. Pathogenesis of simian immunodeficiency virus pneumonia: an immunopathological response to virus. *Am. J. Pathol.* 153: 1123–1130.

Supplemental FIGURE 1

T. Kaneko *et al.*

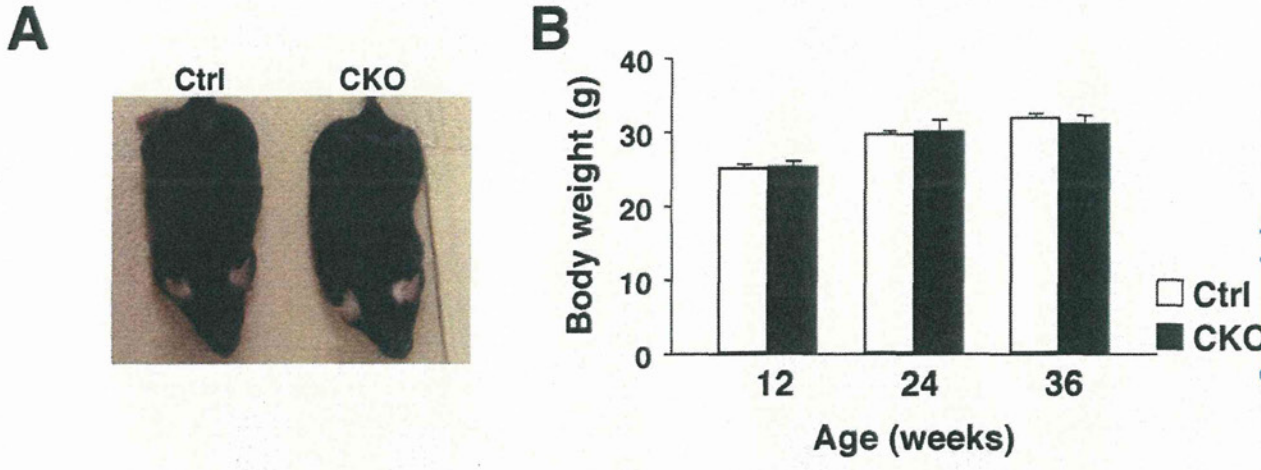

Supple. FIGURE 1. Appearance and Growth of Shp1 CKO Mice. ***A***, Appearance of control and Shp1 CKO mice at 26 wks of age. ***B***, Body weight of control and Shp1 CKO mice at the indicated ages. Data are means ± SE for nine mice of each genotype at each age.

Supplemental FIGURE 2

T. Kaneko *et al.*

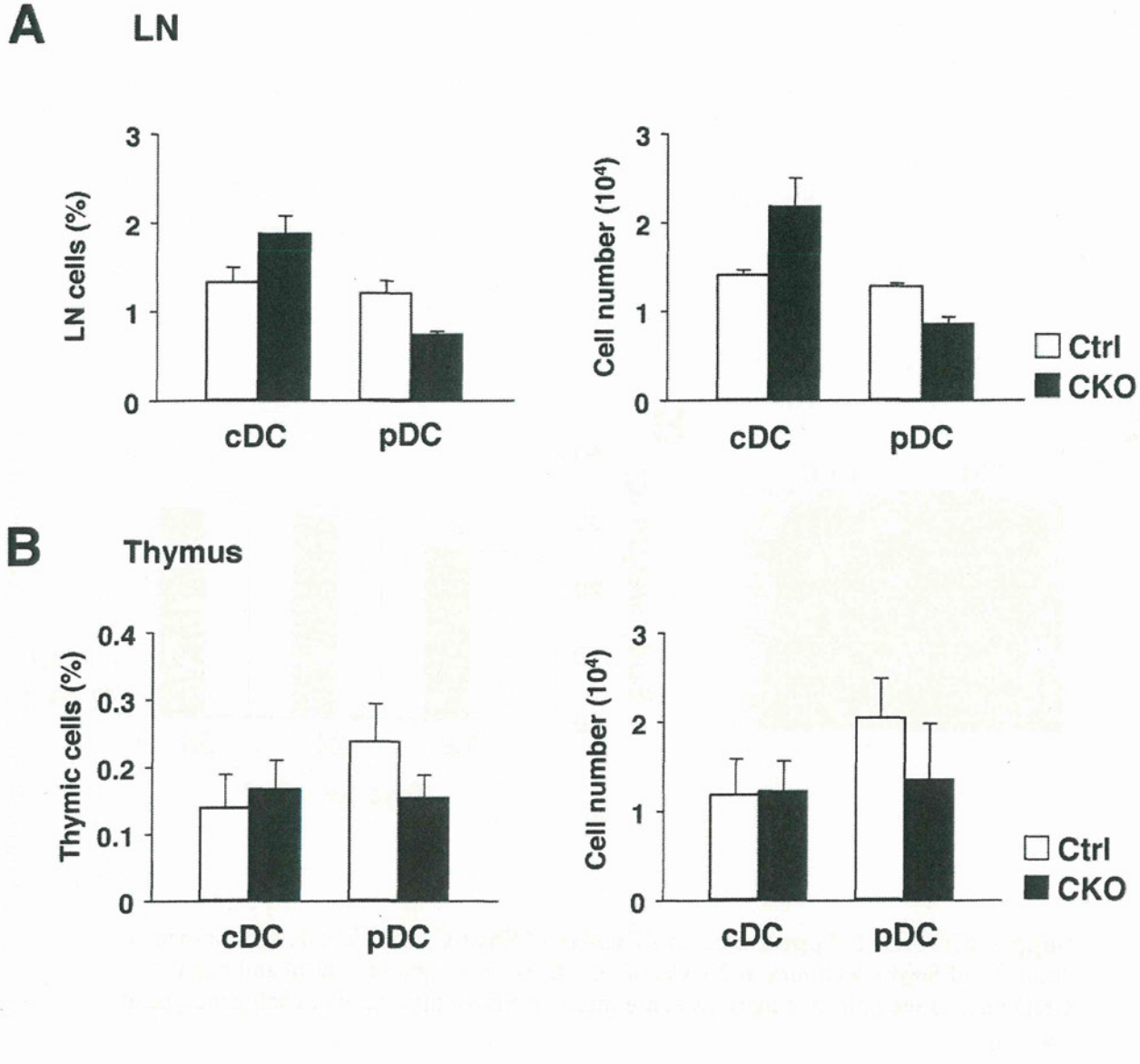

Supple. FIGURE 2. Populations of cDCs and pDCs in Peripheral LNs and the Thymus of Shp1 CKO Mice. Cells prepared from peripheral LNs (*A*) or the thymus (*B*) of control or Shp1 CKO mice at 10 to 12 wks of age were stained for CD11c and B220 as well as with PI and were then analyzed by flow cytometry for determination of the percentages of cDCs and pDCs among total viable cells (left panel) as well as the absolute numbers of these DCs (right panel). Data are means ± SE for three mice per group and are representative of three independent experiments.

Supplemental FIGURE 3

T. Kaneko *et al.*

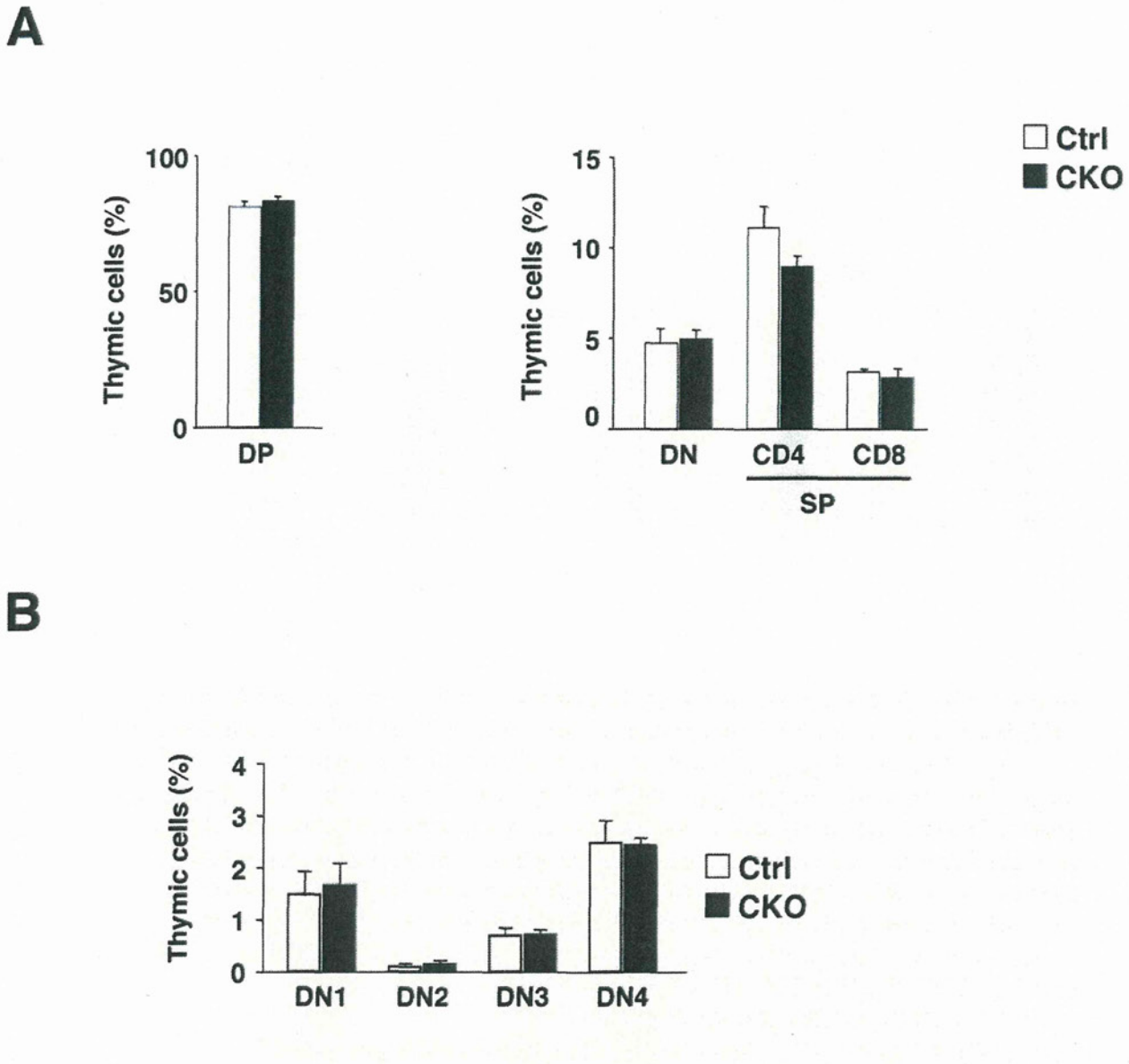

Supple. FIGURE 3. Subpopulations of Thymocytes of Shp1 CKO Mice. ***A***, Cells prepared from the thymus of control or Shp1 CKO mice at 10 to 12 wks of age were stained for CD4, CD8, CD25, and CD44 as well as with PI for analysis by flow cytometry. The percentages of double-positive (DP, $CD4^+CD8^+$; left panel) as well as double-negative (DN, $CD4^-CD8^-$), CD4 single-positive (CD4 SP, $CD4^+CD8^-$), or CD8 SP ($CD4^-CD8^+$) (right panel) thymocytes among PI-negative cells were determined. Data are means ± SE for three mice per group. ***B***, The percentages of DN thymocyte subsets among PI-negative thymocytes were also determined. DN1, $CD44^+CD25^-$; DN2, $CD44^+CD25^+$; DN3, $CD44^-CD25^+$; DN4, $CD44^-CD25^-$. Data are means ± SE for three mice per group.

Supplemental FIGURE 4

T. Kaneko *et al.*

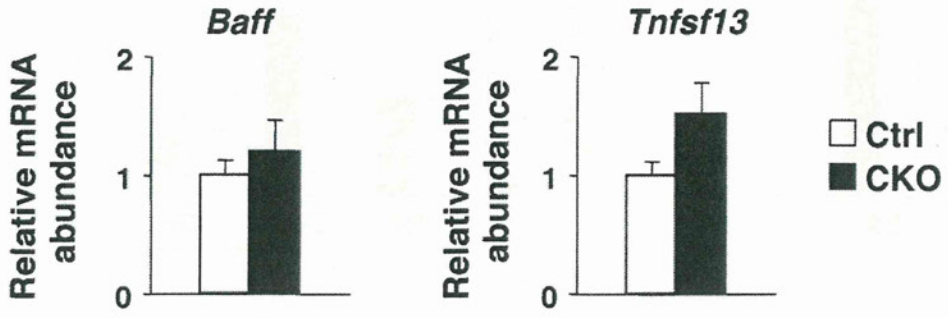

Supple. FIGURE 4. Abundance of BAFF and APRIL mRNAs in Splenic DCs of Shp1 CKO Mice. Total RNA was extracted from isolated splenic CD11c$^+$ DCs of control or Shp1 CKO mice at 12 wks of age with the use of an RNeasy Mini Kit (Qiagen, Valencia, CA), and portions (0.5 μg) of the RNA were subjected to reverse transcription with a QuantiTect Reverse Transcription kit (Qiagen). The resulting cDNA was then subjected to real-time PCR analysis in 96-well plates with specific primers and with the use of a QuantiTect SYBR Green PCR kit (Qiagen), a LightCycler 480 instrument (Roche Diagnostics, Mannheim, Germany), and LightCycler 480 software (Roche Diagnostics). Primer sequences (forward and reverse, respectively) were 5'-ACACTGCCCAACAATTCCTG-3' and 5'-TCGTCTCCGTTGCGTGAAATC-3' for *Baff*, 5'-TCACAATGGGTCAGGTGGTACT-3' and 5'-TGTAAATGAAAGACACCTGCACTGT-3' for *Tnfsf13* (APRIL gene), and 5'-ACCAACTGGGACGACATGGAGAAGA-3' and 5'-TACGACCAGAGGCATACAGGGAC-3' for *Actb* (β-actin gene). The amount of each target mRNA was normalized by that of β-actin mRNA and expressed relative to the value for control mice. Data are means ± SE for six mice per group.

Macrophages require Skap2 and Sirpα for integrin-stimulated cytoskeletal rearrangement

Francis J. Alenghat[1,2], Quentin J. Baca[1], Nooreen T. Rubin[3], Lily I. Pao[4,*], Takashi Matozaki[5], Clifford A. Lowell[6], David E. Golan[1,7,§], Benjamin G. Neel[4,‡,§] and Kenneth D. Swanson[3,4,§]

[1]Department of Biological Chemistry and Molecular Pharmacology, Harvard Medical School, Boston, MA 02115, USA
[2]Cardiovascular Division, Brigham and Women's Hospital, Boston, MA 02115, USA
[3]Division of Signal Transduction, Departments of Medicine and Department of Neurology, Beth Israel Deaconess Medical Center, Boston, MA 02115, USA
[4]Cancer Biology Program, Department of Medicine, Beth Israel Deaconess Medical Center, Boston, MA 02115, USA
[5]Division of Molecular and Cellular Signaling, Department of Biochemistry and Molecular Biology, Kobe University Graduate School of Medicine, 7-5-1 Kusunoki-cho, Chuo-ku, Kobe 650-0017, Japan
[6]Department of Laboratory Medicine, University of California, San Francisco, CA 94143, USA
[7]Hematology Division, Brigham and Women's Hospital, Boston, MA 02115, USA

*Present address: Five Prime Therapeutics Inc., South San Francisco, CA 94080, USA
§Authors for correspondence (david_golan@hms.harvard.edu; bneel@uhnresearch.ca; kswanson@bidmc.harvard.edu)
‡Present address: Campbell Family Cancer Research Institute, Ontario Cancer Institute, Princess Margaret Hospital and Department of Medical Biophysics, University of Toronto, Toronto, Ontario, M5G 1L7, Canada

Accepted 13 August 2012
Journal of Cell Science 125, 5535–5545

doi: 10.1242/jcs.111260

Summary

Macrophages migrate to sites of insult during normal inflammatory responses. Integrins guide such migration, but the transmission of signals from integrins into the requisite cytoskeletal changes is poorly understood. We have discovered that the hematopoietic adaptor protein Skap2 is necessary for macrophage migration, chemotaxis, global actin reorganization and local actin reorganization upon integrin engagement. Binding of phosphatidylinositol [3,4,5]-triphosphate to the Skap2 pleckstrin-homology (PH) domain, which relieves its conformational auto-inhibition, is critical for this integrin-driven cytoskeletal response. Skap2 enables integrin-induced tyrosyl phosphorylation of Src-family kinases (SFKs), Adap, and Sirpα, establishing their roles as signaling partners in this process. Furthermore, macrophages lacking functional Sirpα unexpectedly have impaired local integrin-induced responses identical to those of *Skap2*$^{-/-}$ macrophages, and Skap2 requires Sirpα for its recruitment to engaged integrins and for coordinating downstream actin rearrangement. By revealing the positive-regulatory role of Sirpα in a Skap2-mediated mechanism connecting integrin engagement with cytoskeletal rearrangement, these data demonstrate that Sirpα is not exclusively immunoinhibitory, and illuminate previously unexplained observations implicating Skap2 and Sirpα in mouse models of inflammatory disease.

Key words: Cytoskeleton, Inflammation, Integrin, Macrophage, Migration

Introduction

To participate in inflammatory responses, macrophages and their precursors must migrate to perceived sites of infection or insult (Geissmann et al., 2010; Hume, 2006). These cells rely on cues from the local environment delivered through integrins, receptors critical for cell-matrix and cell-cell interactions (Berton and Lowell, 1999; Hynes, 2002). Inflammatory stimuli can induce "inside-out" signals that control integrin cell surface expression and affinity for extracellular ligands. In turn, upon ligand binding, integrins initiate "outside-in" signals that control multiple downstream pathways required for cell adhesion, migration, and chemotaxis, all key components of innate and adaptive immune responses (Berton and Lowell, 1999; Gahmberg et al., 1998). These integrin-mediated responses also depend on the macrophage's ability to remodel its cytoskeleton, thereby allowing changes in cell shape, motility, and directionality (Vicente-Manzanares and Sánchez-Madrid, 2004; Worthylake and Burridge, 2001). Despite their central role in macrophage function, the mechanisms by which integrin signals lead to cytoskeletal reorganization remain unclear.

In leukocytes, adaptor proteins participate in integrin-driven signaling. One such protein, Src kinase-associated phosphoprotein 2 (Skap2, a.k.a. Skap-hom), interacts with Adhesion and Degranulation-Promoting Adapter Protein (Adap, a.k.a. Fyb), an established integrin-responsive protein (Kasirer-Friede et al., 2007). Moreover, integrin engagement induces tyrosyl phosphorylation of Skap2 and Adap (Timms et al., 1999). The structurally similar Skap1 is expressed specifically in T cells and also binds Adap. However, Skap2 is expressed broadly in lymphoid and myeloid cells (Kouroku et al., 1998; Liu et al., 1998; Marie-Cardine et al., 1998) and cannot substitute for Skap1 in regulating T cell inside-out signals (Griffiths et al., 2001; Jo et al., 2005; Moog-Lutz et al., 2001), suggesting that Skap2 may perform a distinct role during integrin signaling. Studies have suggested an adhesive/migratory role for Skap2 in B cells and dendritic cells, but have provided no mechanism or relationship to integrin engagement or cytoskeleton modulation (Reinhold et al., 2009; Togni et al., 2005). Indeed, how Skap2 functions at the molecular level is not well understood in any biological system.

Skap2 also binds the transmembrane protein Signal Regulatory Protein-α (Sirpα, a.k.a. SHPS-1), which is generally regarded as an immune inhibitory receptor (Barclay, 2009; Kharitonenkov et al., 1997; Veillette et al., 1998). Like Skap2, Sirpα is tyrosyl phosphorylated in response to integrin engagement in macrophages (Inagaki et al., 2000; Johansen and Brown, 2007; Motegi et al., 2003; Timms et al., 1999). Importantly, Skap2- and Sirpα-deficient mice are resistant to autoimmune processes, such as experimental autoimmune encephalomyelitis (EAE) and collagen-induced arthritis, which serve as models for human disease (multiple sclerosis and rheumatoid arthritis) that have integrin-dependent components (Okuzawa et al., 2008; Ransohoff, 2007; Togni et al., 2005; Tomizawa et al., 2007). Indeed integrins have emerged as important therapeutic targets in multiple sclerosis, rheumatoid arthritis, and other autoimmune diseases, such as inflammatory bowel disease (Parikh et al., 2012; Peters et al., 2011; Ransohoff, 2007; Rutgeerts et al., 2009). Thus, determining whether Skap2 and Sirpα regulate macrophage responses to integrin signals could significantly enhance our mechanistic understanding of inflammatory responses and diseases, thereby facilitating the identification of new therapeutic targets. Here, we find that Skap2 and Sirpα drive the transduction of integrin-evoked signals that lead to the cytoskeletal rearrangement required for macrophage migration.

Results

Skap2 is required for macrophage migration, chemotaxis, and spreading

To determine whether Skap2 is required for migration, we tested the ability of bone marrow-derived macrophages (BMMs) from *Skap2*$^{-/-}$ mice to migrate into scratches introduced into densely populated cultures. *Skap2*$^{-/-}$ BMMs exhibited a pronounced migration defect in this assay (Fig. 1A). Likewise, these cells showed decreased migratory responses driven by M-CSF or the chemokines CCL2 and CXCL4 in transwell assays (Fig. 1B–D). *Skap2*$^{-/-}$ BMMs also spread poorly on glass, which binds BMMs predominantly through their β2 integrins (Brown, 1991; Yakubenko et al., 2002), and impaired BMM spreading was accompanied by reduced F-actin content as measured by phalloidin staining (Fig. 1E,F). Together, these results suggest a mechanism in which Skap2 is necessary for eliciting the cytoskeletal changes that drive macrophage motility.

The spreading and migratory defects were observed in the absence of chemokine/cytokine gradients, suggesting that processes downstream of integrin engagement, not cytokine or chemokine detection *per se*, were affected by the loss of Skap2. Indeed, *Skap2*$^{-/-}$ BMMs proliferate normally in response to M-CSF and GM-CSF (Togni et al., 2005), and M-CSF-induced tyrosyl phosphorylation was not globally perturbed by Skap2 deficiency (Fig. 2A). Although lysates from M-CSF-stimulated *Skap2*$^{-/-}$ BMMs showed the absence of a ~50 kD phosphotyrosyl band that was observed in M-CSF-treated *Skap2*$^{+/-}$ BMMs, this band primarily corresponded to Skap2 itself (Bourette et al., 2005), as demonstrated by immunodepletion experiments (supplementary material Fig. S1). *Skap2*$^{-/-}$ BMMs also had normal integrin expression, so their defective migration and spreading were not due to decreased integrin availability (Fig. 2B). Furthermore, flow cytometric analysis with the activation-specific antibody 9EG7 showed similar levels of basal and phorbol 12-myristate 13-acetate (PMA)-evoked β1 integrin activation in WT and *Skap2*$^{-/-}$ BMMs, suggesting that inside-out integrin activation was not impaired in these cells (supplementary material Fig. S2).

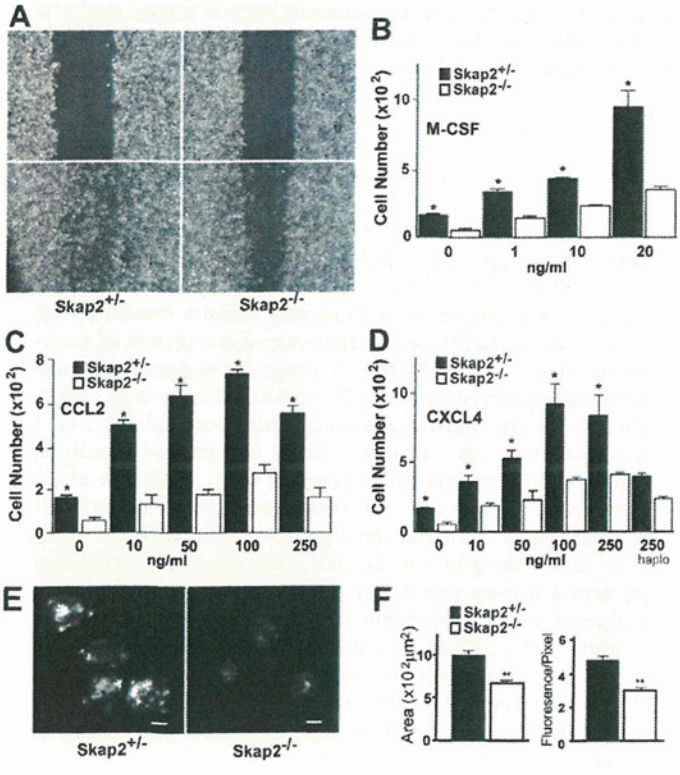

Fig. 1. Skap2-deficient BMMs exhibit defective migration, spreading, and actin polymerization. (A) Scratches were introduced into confluent cultures of *Skap2*$^{+/-}$ or *Skap2*$^{-/-}$ BMMs (upper panels). After 8 hours (lower panels), migration across the scratch wounds was impaired in cells lacking Skap2. (**B–D**) Chemotaxis of *Skap2*$^{+/-}$ and *Skap2*$^{-/-}$ BMMs in response to cytokine M-CSF (B) and chemokines CCL2 (C) and CXCL4 (D) in transwell migration assays. In D, "haplo" denotes haplotaxis conditions where equal concentrations of CXCL4 are in both chambers. For B–D, data are presented as mean ± S.E.M., $n=3$, $^{*}P<0.01$ compared to *Skap2*$^{-/-}$ under the same condition. (**E**) *Skap2*$^{+/-}$ or *Skap2*$^{-/-}$ BMMs were suspended in DMEM for 3 hours, plated for 30 minutes on glass coverslips, then fixed and stained for F-actin with rhodamine-labeled phalloidin. Scale bar: 10 μm. (**F**) Quantification of plating-induced spreading area from (E) in μm^2 (left) and relative fluorescence intensity per pixel for rhodamine-labeled phalloidin (right) for *Skap2*$^{+/-}$ and *Skap2*$^{-/-}$ BMMs. Data presented as mean ± S.E.M., $n=30$, $^{**}P<0.001$ compared to *Skap2*$^{+/-}$ BMMs.

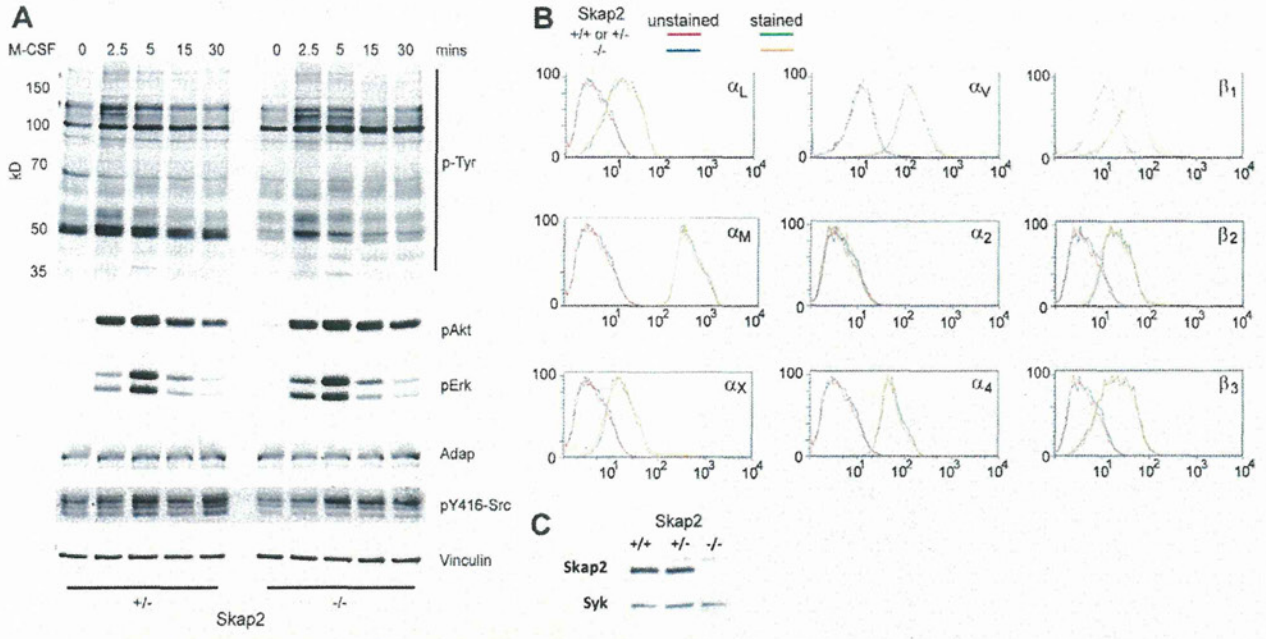

Fig. 2. Skap2 is not required for M-CSF-induced signaling and does not affect integrin expression in macrophages. (**A**) Adherent *Skap2*$^{+/-}$ and *Skap2*$^{-/-}$ BMMs treated with M-CSF for the indicated times were lysed, electrophoresed, and immunoblotted for phosphotyrosine (p-Tyr) and phosphorylated Akt, Erk2, and Src, with total Adap and Vinculin as loading controls. (**B**) Flow cytometric analysis was performed on Skap2-replete (WT, except *Skap2*$^{+/-}$ for α_V and β_1) or *Skap2*$^{-/-}$ BMMs using antibodies against the indicated cell surface integrins. (**C**) *Skap2*$^{+/+}$ and *Skap2*$^{+/-}$ BMMs express equal amounts of Skap2 protein; Syk is a loading control. For all panels, representative results from two independent experiments are shown.

Notably, *Skap2*$^{+/-}$ BMM responses were identical to those of wild-type (WT, *Skap2*$^{+/+}$) BMMs in our assays; this was likely due to the role Adap plays in binding and stabilizing Skap1 and Skap2 against proteolysis (Huang et al., 2005; Kasirer-Friede et al., 2007), thereby limiting Skap2's intracellular expression (Togni et al., 2005), which was equivalent in WT and *Skap2*$^{+/-}$ BMMs (Fig. 2C). Indeed, immunodepletion of Skap2 from lysates of *Skap2*$^{+/-}$ cells also resulted in depletion of Adap (Timms et al., 1999; supplementary material Fig. S1), suggesting that the level of protein produced by a single *Skap2* allele was able to saturate the available Adap.

Skap2 is required for integrin-dependent actin cytoskeletal rearrangement

Because Skap2 is crucial for macrophage migration, chemotaxis, and spreading, we hypothesized that it is required for integrin-dependent actin cytoskeletal rearrangement. After spreading on glass, *Skap2*$^{+/-}$ BMMs developed pronounced actin ruffles, or curvilinear accumulations of polymerized F-actin (Fig. 3A). By contrast, *Skap2*$^{-/-}$ BMMs developed fewer and shorter ruffles (Fig. 3B). In *Skap2*$^{+/-}$ BMMs, Skap2 colocalized with ruffles preferentially at the leading edges and apical portions of the cells (Fig. 3C), often within punctate structures associated with the edges of ruffles. Trails of subjacent actin were observed to emanate from the ruffles' leading edges (supplementary material Movie 1).

Cell adhesion, migration, and chemotaxis are complex processes that integrate changes in integrin modulation and engagement, cytoskeletal reorganization, cell polarization, and cell shape through interconnected signaling pathways (Berzat and Hall, 2010; Chen et al., 2003; Jones, 2000). In the face of such complexity, it is advantageous to study integrin-mediated events through spatially and temporally focused approaches in model systems that isolate and control receptor engagement in order to measure local, early responses. Therefore, we employed a bead assay that incorporated integrin ligands and monoclonal antibodies to examine further the role of Skap2 in integrin-mediated cytoskeletal rearrangement. Polystyrene beads were coated with polyRGD (pRGD) (Alenghat et al., 2009; Miyamoto et al., 1995), which binds to a broad range of integrins, including β_1, β_2, and β_3 (Plow et al., 2000). *Skap2*$^{+/-}$ and *Skap2*$^{-/-}$ BMMs bound these beads similarly, consistent with their equivalent levels of surface integrin expression (Fig. 2B). However, whereas pRGD beads evoked pronounced actin ruffling in *Skap2*$^{+/-}$ BMMs (Fig. 3D), *Skap2*$^{-/-}$ BMMs generated markedly less ruffling in proximity to the beads (Fig. 3E,F). This cytoskeletal response occurred within 20 minutes of integrin engagement, and beads coated with a control protein (albumin) failed to elicit ruffling in BMMs of either genotype (Fig. 3F). Finally, a monoclonal antibody directed against the extracellular portion of α_V integrin, which, by clustering integrins, evokes signaling, yielded similar results (Fig. 3F). As with the ruffles seen in plated cells, Skap2 was concentrated at the leading edges of these integrin-induced actin structures (supplementary material Movie 2).

Manganese (Mn^{2+}), which activates integrins non-selectively (Dransfield et al., 1992), enhanced the cytoskeletal response to control beads in Skap2-replete cells, but had no detectable additional effect on local integrin-mediated ruffling in response to pRGD-coated beads in either *Skap2*$^{+/-}$ or *Skap2*$^{-/-}$ cells (Fig. 3G). Moreover, the requirement for Skap2 for integrin-induced actin ruffling was generalizable across several other α

and β integrins found on macrophages (Fig. 3H). From these studies, we concluded that Skap2 plays a general and essential role in integrin-mediated actin rearrangements in BMMs.

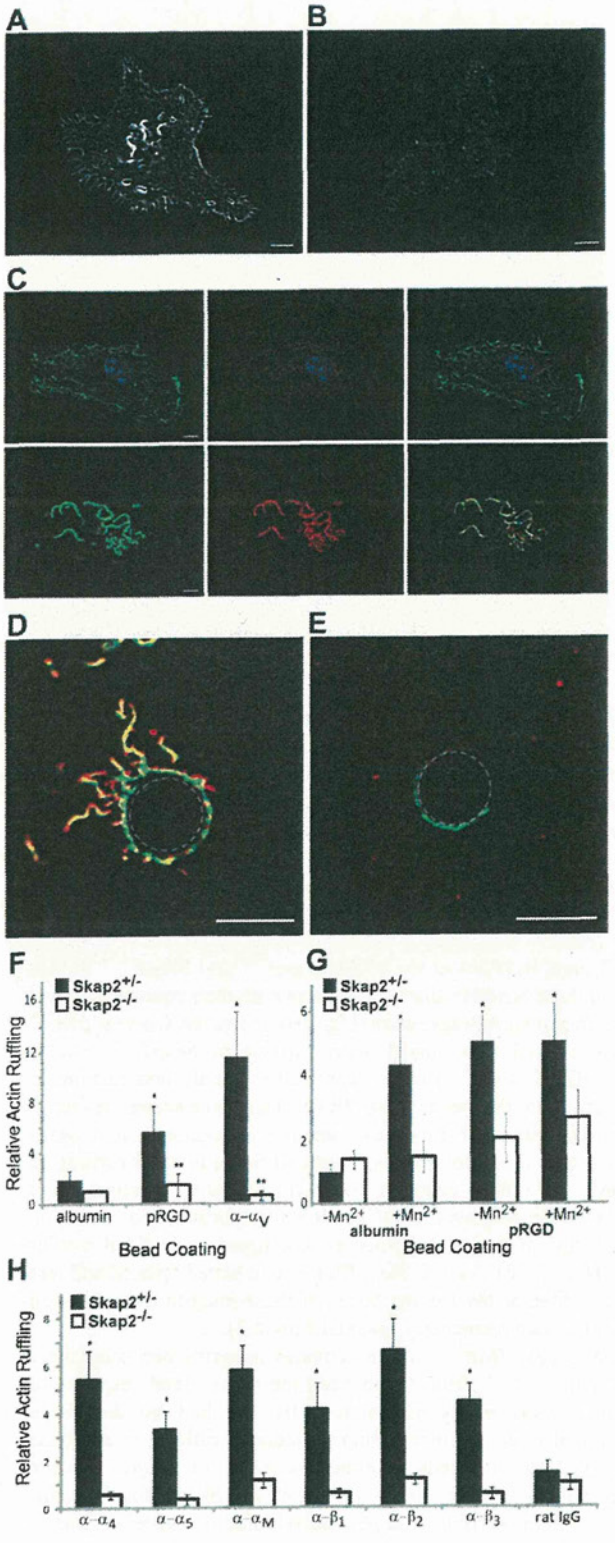

Skap2 structural domains determine integrin-induced signaling

Structural and functional studies have shown that unstimulated Skap2 exists in an auto-inhibited state, wherein the pleckstrin-homology (PH) domain binds to a four-helix bundle created by the interaction of N-terminal dimerization domains (DM) of Skap2 monomers, and that this auto-inhibitory interaction is relieved upon phosphatidylinositol [3,4,5]-triphosphate (PIP3) binding (Swanson et al., 2008). To probe the role of specific Skap2 domains in regulating integrin-mediated cytoskeletal responses, we reconstituted *Skap2*$^{-/-}$ BMMs with Skap2 mutants that either disrupt the auto-inhibitory DM/PH domain interaction (D129K) or impair PIP3 binding (R140M) (Swanson et al., 2008). WT Skap2 rescued the deficient actin ruffling of *Skap2*$^{-/-}$ BMMs (Fig. 4A). However, expression of the R140M mutant in *Skap2*$^{-/-}$ BMMs failed to rescue integrin-induced ruffling (Fig. 4A). Furthermore, expression of this mutant, which dimerizes with normal Skap2 in Skap2-replete BMMs (Swanson et al., 2008), completely prevented the normal response in a dominant negative fashion (Fig. 4B). Preventing PIP3 production with the PI3K inhibitor GSK2126458 (Leung et al., 2011) also ablated the ruffling response (supplementary material Fig. S3A). By contrast, superimposing the D129K mutation on R140M (D129K/R140M) led to hyperactive actin polymerization beyond the level generated by WT Skap2 (Fig. 4A), and even generated a significant response to control beads (likely through non-specific integrin interactions with polystyrene (Brown, 1991; Yakubenko et al., 2002). This hyperactive response occurred despite the inability of this mutant to bind PIP3 (as a consequence of the R140M mutation), indicating that the auto-inhibitory DM/PH domain interaction is a critical regulator of Skap2 action. Consistent with this conclusion, mutation of D129K alone also evoked hyperactive actin polymerization (supplementary

Fig. 3. Skap2 is required for integrin-dependent actin cytoskeletal rearrangement. (**A**) Confocal micrograph of a typical phalloidin-stained *Skap2*$^{+/-}$ BMM plated on glass, demonstrating curvilinear actin ruffles. (**B**) *Skap2*$^{-/-}$ BMMs typically exhibit less actin ruffle formation. (**C**) At the plane of the nucleus (top panels, with blue nucleus in focus), a *Skap2*$^{+/-}$ BMM has minimal cortical actin (green) and cytosolic Skap2 (red), without significant colocalization (yellow, in merge); in contrast, at the apical surface (bottom panels), Skap2 colocalizes strongly with cortical actin ruffles. See also supplementary material Movie 1. (**D**) Upon binding to a *Skap2*$^{+/-}$ BMM for 20 minutes, a polystyrene bead (denoted by dotted outline) coated with anti-α_V integrin antibodies recruits actin ruffles (green) colocalized with Skap2 (red). See also supplementary material Movie 2. (**E**) This response is markedly reduced in *Skap2*$^{-/-}$ BMMs. Scale bar: 10 μm.
(**F**) Quantified actin ruffling responses, measured as average pixel intensity in an 8-μm annulus surrounding beads coated with integrin-engaging or control proteins, are shown for BMMs of both genotypes. Data are normalized against the albumin/*Skap2*$^{-/-}$ condition as Relative Actin Ruffling and presented as mean ± S.E.M., $n=10$ per condition, $^{*}P<0.05$ compared to albumin-coated beads on the same cells, $^{**}P<0.01$ compared to same beads on *Skap2*$^{+/-}$ BMMs. (**G**) Quantified actin ruffling responses, induced by binding to polystyrene beads coated with either albumin or polyRGD, is shown for *Skap2*$^{+/-}$ and *Skap2*$^{-/-}$ BMMs with or without treatment with 1 mM Mn^{2+}. Data are normalized against the Mn^{2+}/albumin/*Skap2*$^{+/-}$ condition and presented as mean ± S.E.M., $n=10$ per condition, $^{*}P<0.05$ compared to albumin-coated beads, no Mn^{2+}, on the same cells. (**H**) Quantified actin ruffling responses to subtype-specific integrin-engaging beads are shown for BMMs of both genotypes. Data are normalized against the rat IgG/*Skap2*$^{-/-}$ condition and presented as mean ± S.E.M., $n=10$ per condition, $^{*}P<0.01$ compared to the same beads on *Skap2*$^{-/-}$ BMMs.

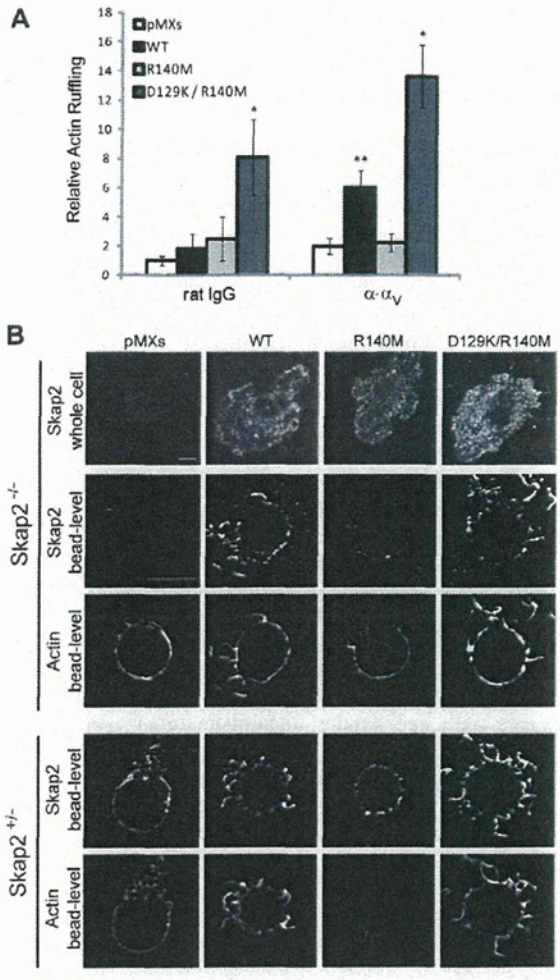

Fig. 4. Integrin-induced cytoskeletal reorganization requires a functional Skap2 PH domain. (**A**) Actin ruffling induced by beads coated with rat IgG (control) or anti-α_V bound to *Skap2*$^{-/-}$ BMMs infected with empty vector (pMXs), WT Skap2 (WT), or Skap2 mutants with an R140M substitution or with combined D129K and R140M substitutions. Data are presented as mean ± S.E.M., $n=10$ per condition, $*P<0.01$ compared to pMXs, $**P<0.05$ compared to pMXs. (**B**) *Skap2*$^{-/-}$ and *Skap2*$^{+/-}$ BMMs infected with empty vector (pMXs), WT Skap2 (WT), or Skap2 mutants with an R140M substitution or with combined D129K and R140M substitutions were bound to polystyrene beads coated with antibodies directed against α_V integrin, and stained for actin (phalloidin) and for Skap2. $n=10$ per condition. Scale bar: 10 μm.

material Fig. S3B). These data indicated that relief of auto-inhibition via PIP3 binding to the Skap2 PH domain is critical for Skap2 function in integrin-mediated cytoskeletal reorganization in BMMs; they further showed that the normal auto-inhibitory interaction – between the Skap2 PH and DM domains – is required for regulating the integrin-driven actin response in these cells.

Skap2 directs a subset of integrin-induced Sirpα-associated signaling events

The observed defects in integrin mobility, cytoskeletal rearrangement, and migration in *Skap2*$^{-/-}$ BMMs led us to investigate the effect of Skap2 deficiency on integrin-stimulated signaling. BMMs were plated onto fibrinogen-coated surfaces in order to trigger integrin (primarily β_2 and β_3) activation. Plating-induced protein tyrosyl phosphorylation was globally decreased in the absence of Skap2, consistent with a defect in an early event in integrin signal transduction (Fig. 5A). Indeed, activation of SFK was abrogated in the absence of Skap2 (Fig. 5A). Although there was a mild decrement in the residual low level of SFK activation seen in suspended *Skap2*$^{-/-}$ cells compared with control cells, this did not appear to affect the basal integrin activation state (supplementary material Fig. S2). Notably, Mn^{2+} restored global integrin-evoked tyrosyl phosphorylation as well as SFK activation in *Skap2*$^{-/-}$ BMMs (Fig. 5A); this is significant because Mn^{2+} was unable to restore integrin-induced actin ruffling in these cells (Fig. 3G). Therefore, the Mn^{2+}-induced tyrosyl-phosphorylated proteins in Skap2-deficient cells likely represent participants in pathways distinct from those leading to the Skap2-dependent actin ruffling response. Likewise, whereas basal Syk phosphorylation was mildly increased in *Skap2*$^{-/-}$ cells, plating-induced tyrosyl phosphorylation of Syk, an established integrin effector required for cytoskeletal rearrangement (Vines et al., 2001), was not affected significantly by the absence of Skap2, and, like SFK activity, was amplified by Mn^{2+} treatment in both *Skap2*$^{+/-}$ and *Skap2*$^{-/-}$ cells (Fig. 5B). These results demonstrate that, while activated integrins can stimulate SFKs and Syk, even forced activation of these proteins with Mn^{2+} was insufficient to drive actin rearrangement in the absence of Skap2.

Adap, a known binding partner of Skap2, failed to become tyrosyl phosphorylated in response to integrin engagement in *Skap2*$^{-/-}$ BMMs; moreover, in contrast to the SFK and Syk results, Mn^{2+}-induced Adap phosphorylation was minimal and failed to reach the levels of Adap phosphorylation found in control cells (Fig. 5C). Therefore, although Skap2 participates in inside-out integrin activation of SFKs, activation of a specific Skap2 signaling partner (Adap), along with downstream actin remodelling, is driven primarily through Skap2-mediated outside-in signaling. Similar results were obtained when BMMs were plated on fibronectin (not shown), which primarily engages β_1 and β_3 integrins, again indicating that Skap2 propagates signals downstream of multiple integrins.

We have shown previously that the transmembrane receptor Sirpα forms complexes with Skap2 and Pyk2 independently of Sirpα tyrosyl phosphorylation and Shp1/2 binding (Timms et al., 1999). Furthermore, inhibition of Sirpα function can lead to defects in cell migration (Inagaki et al., 2000; Motegi et al., 2003). Whereas both Sirpα and Sirpα-associated Pyk2 became tyrosyl phosphorylated in *Skap2*$^{+/-}$ BMMs plated on integrin ligands, plating-induced phosphorylation of Sirpα was minimal in *Skap2*$^{-/-}$ BMMs (Fig. 5D). By contrast, activation of Pyk2, another binding partner of Sirpα (Timms et al., 1999), was not affected by Skap2 deficiency. As with Adap, Sirpα phosphorylation, which occurs within the immunoreceptor tyrosine-based inhibitory motifs (ITIMs), was not salvaged by Mn^{2+} treatment of *Skap2*$^{-/-}$ cells (Fig. 5D), suggesting that this event, but not Pyk2 activation, is part of a Skap2-dependent outside-in pathway. This model is consistent with the finding that Skap2 and Pyk2 associate with separate pools of Sirpα (Timms et al., 1999), and with our observation that plating-induced activation of Akt, Erk, and Paxillin (all Pyk2 effectors) was not altered in *Skap2*$^{-/-}$ BMMs (Fig. 5E) (Blaukat et al., 1999; Williams and Ridley, 2000). Interestingly, *Lyn*$^{-/-}$ BMMs showed a similar defect in Sirpα phosphorylation with normal

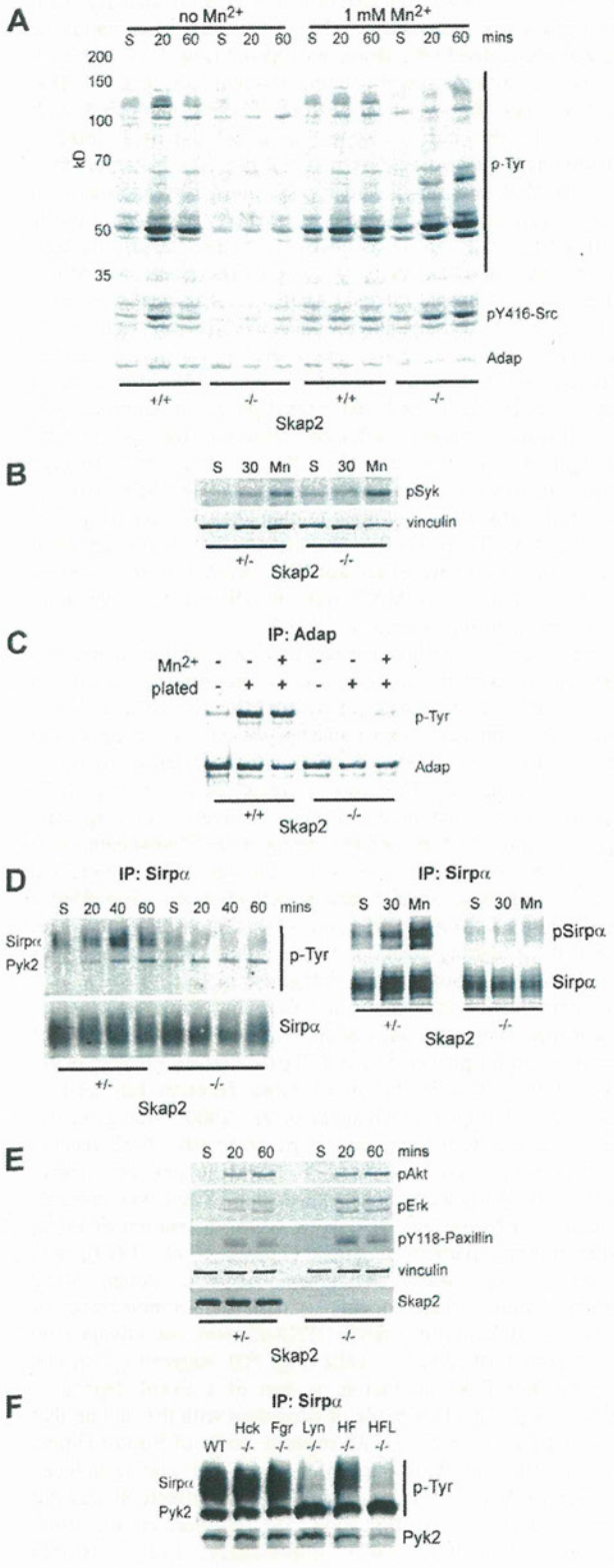

Pyk2 phosphorylation upon plating-induced integrin engagement (Fig. 5F; supplementary material Fig. S4), implicating Lyn as the primary SFK involved downstream of Skap2 in pathways leading to Sirpα phosphorylation (Hibbs et al., 2002).

Sirpα also is necessary for the Skap2-dependent cytoskeletal response

Skap2 binds to Sirpα and directs its integrin-dependent phosphorylation, but does not control other aspects of integrin-dependent Sirpα signaling (see above). These results led us to further probe Sirpα's role in integrin-induced cytoskeletal rearrangement. As in *Skap2*$^{-/-}$ cells, BMMs from mice homozygous for a Sirpα mutant lacking its cytoplasmic tail [*Sirpα*$^{\Delta/\Delta}$ (Inagaki et al., 2000)] exhibited deficient actin ruffling in response to integrin ligation by beads coated with either pRGD or α–α_V (Fig. 6A). Like *Skap2*$^{+/-}$ BMMs, *Sirpα*$^{+/\Delta}$ BMM responses were similar to that seen for WT cells. Furthermore, just as in Skap2-deficient cells, the response to integrin ligation was not augmented significantly by Mn^{2+} in *Sirpα*$^{\Delta/\Delta}$ BMMs (Fig. 6B). The normal response of *Sirpα*$^{+/\Delta}$ cells suggested that the mutant Sirpα fragment did not interfere with the function of endogenous wild-type Sirpα. To test this further, we identified two shRNA sequences that depleted Sirpα expression to ~25% of wild-type levels, as demonstrated by immunofluorescence microscopy and by immunoblotting (Fig. 6C). Importantly, cytoskeletal rearrangements in response to bead-based integrin engagement exhibited similar impairment to that seen in the *Sirpα*$^{\Delta/\Delta}$ BMMs (Fig. 6D). These results show that the Sirpα mutation behaves as a null allele for these integrin-dependent functions, and, along with the Skap2-dependent phosphorylation of Sirpα (Fig. 5D), support a cooperative mechanism between Skap2 and Sirpα in driving the actin response.

Fig. 5. Skap2 is required for specific integrin-induced signaling events. (**A**) *Skap2*$^{+/+}$ and *Skap2*$^{-/-}$ BMMs in suspension (S) or plated on fibrinogen for 20 or 60 minutes, either in the absence (left six lanes) or presence (right six lanes) of 1 mM Mn^{2+}, were lysed, electrophoresed and immunoblotted for phosphotyrosine (p-Tyr; upper panel), Src pY416 (middle panel), and Adap as a loading control (lower panel). (**B**) *Skap2*$^{+/-}$ and *Skap2*$^{-/-}$ BMMs were kept in suspension or plated on fibrinogen for 30 minutes in the absence or presence of Mn^{2+}, lysed, and immunoblotted for pSyk and vinculin as a loading control. Baseline quantified pSyk/vinculin is ~2-fold higher in *Skap2*$^{-/-}$ cells. Plating increases levels ~2-fold and Mn^{2+} increases levels ~5-fold in both genotypes. (**C**) *Skap2*$^{+/+}$ and *Skap2*$^{-/-}$ BMMs were kept in suspension or plated on fibrinogen for 30 minutes in the absence or presence of Mn^{2+}, lysed, immunoprecipitated for Adap, and immunoblotted for phosphotyrosine (pTyr; upper panel) and Adap (lower panel). Baseline quantified pTyr/Adap is ~5-fold higher in *Skap2*$^{+/-}$ cells. Plating increases levels ~5-fold in *Skap2*$^{+/-}$ and ~1.2-fold in *Skap2*$^{-/-}$ cells. Mn^{2+} increases levels ~6-fold in *Skap2*$^{+/-}$ cells and 3-fold in *Skap2*$^{-/-}$ cells. (**D**) Sirpα was immunoprecipitated from lysates of BMMs in suspension (S) or after plating for the indicated times on fibrinogen, and phosphotyrosine (p-Tyr) was analyzed by immunoblotting (left panels), with prominent bands corresponding to Sirpα and Pyk2. Similar lysates of suspended, plated, or 1 mM Mn^{2+}-treated BMMs (right panels) were probed for Sirpα phosphorylation. (**E**) Akt, Erk, and Paxillin phosphorylation were probed in *Skap2*$^{+/-}$ and *Skap2*$^{-/-}$ BMMs in suspension (S) or after plating for the indicated times on fibrinogen. (**F**) BMMs from *Hck*$^{-/-}$, *Fgr*$^{-/-}$, and *Lyn*$^{-/-}$, as well as Hck/Fgr double knockout (*HF*$^{-/-}$) and Hck/Fgr/Lyn triple knockout (*HFL*$^{-/-}$) mice, were lysed after plating on fibrinogen, subjected to immunoprecipitation for Sirpα, and immunoblotted for p-Tyr and Pyk2. All panels are representative of at least three independent experiments.